High-spin states in doubly odd ^{166}Tm

M. A. Cardona, [1,2,3] D. Hojman, [1,3] M. E. Debray, [1,2] A. J. Kreiner, [1,2,3] M. Davidson, [1,3] J. Davidson, [1,3] D. R. Napoli, [4]
D. Bazzacco, [5] N. Blasi, [6] S. M. Lenzi, [5] G. Lo Bianco, [7] and C. Rossi Alvarez[5]

[1]*Departamento de Física, Comisión Nacional de Energía Atómica, 1429 Buenos Aires, Argentina*
[2]*Escuela de Ciencia y Tecnología, Universidad de San Martín, Argentina*
[3]*CONICET, 1033 Buenos Aires, Argentina*
[4]*INFN, Laboratori Nazionali di Legnaro, Legnaro, Italy*
[5]*Dipartimento di Fisica, Sezione di Padova, Padova, Italy*
[6]*Dipartimento di Fisica and INFN, Sezione di Milano, Milano, Italy*
[7]*Dipartimento di Matematica e Fisica, Università di Camerino, Italy*

High-spin states in doubly odd ^{166}Tm were investigated by means of in-beam γ-ray spectroscopy techniques using the multidetector array GASP. Excited states of ^{166}Tm were populated using the ^{160}Gd(^{11}B,5n) reaction at a beam energy of 61 MeV. Known rotational bands have been extended to higher spins and their configurations have been discussed. Alignments, band crossing frequencies, and electromagnetic properties have been analyzed in the framework of the cranking model. Signature inversion in the $\pi h_{9/2} \otimes \nu i_{13/2}$ structure is discussed. Calculations in the framework of the particle rotor model with $p-n$ interaction included have been able to reproduce the inversion. $E1$ decay modes were observed in competition with $E2$ intraband transitions.

I. INTRODUCTION

The study of doubly odd nuclei has provided a fruitful ground for the discovery and discussion of a number of interesting nuclear structure phenomena [1]. One recurrent theme has been the identification and classification of the structures of the rotational bands among the multitude of the possible combinations of proton and neutron configurations which occur at low excitation energy [1,2]. To this aim a firm determination of spins, parities, and excitation energies associated with the rotational bands is very helpful. A variety of interesting phenomena has been discovered along the way, among them that of signature inversion [3,4]. This feature has been recently observed in the $\pi h_{9/2} \otimes \nu i_{13/2}$ structure, often called semidecoupled [5], and its origin discussed in terms of the proton-neutron residual interaction [6,7]. The present study of the doubly odd ^{166}Tm is framed into the above context. This nucleus has been reexamined using the GASP detector array at the Legnaro Tandem Facility yielding a wealth of rotational structures where the abovementioned ideas can be tested. In particular the large amount of high quality triple γ-ray coincidence data allows the observation of multiple interband transitions leading to more accurate spin and parity assignments. The $\pi h_{9/2} \otimes \nu i_{13/2}$ semidecoupled structure was identified exhibiting signature inversion. In this band $E1$ decay modes were observed in competition with $E2$ intraband transitions. For example, pronounced $E1$ decays into the $\pi 1/2^+[411] \otimes \nu i_{13/2}$ band were established over a large spin range. The strength of these $E1$ transitions was compared along the isotopic chain ^{162,164}Tm [8,9] and ^{166}Tm. Moreover, $E1$ decays into the $\pi h_{9/2} \otimes \nu 5/2^-[523]$ were identified.

The ^{166}Tm nucleus has been studied earlier using the $(\alpha,3n)$ reaction [10–12]. In Ref. [12] a level scheme containing several rotational bands was carefully constructed. In this last work, the authors used an online crystal spectrometer which was crucial for establishing the placement of several γ rays, helping in the construction of the complicated low-spin part of the level scheme. Other investigations which include magnetic moment measurements [13–16] have established $I^\pi = 2^+$ and the configuration $\pi 1/2^+[411] \otimes \nu i_{13/2}(5/2^+[642])$ for the ground state of ^{166}Tm. In Ref. [17] a long lived isomeric state ($T_{1/2} = 340$ ms) was established and identified as the bandhead of the $7/2^+[404] \otimes \nu 5/2^-[523]K^\pi = 6^-$ structure. The works of Refs. [12] and [17] were very useful in the present investigation.

II. EXPERIMENTS AND RESULTS

A. Measurements

High-spin states of ^{166}Tm were populated through the ^{160}Gd(^{11}B,5n) reaction at 61 MeV. In this experiment the beam was provided by the Tandem XTU accelerator of Legnaro and was focused on a stack of three foils. Each foil consisted of 180 μg/cm^2 isotopically enriched ^{160}Gd$_2$O$_3$ evaporated onto a 15 μg/cm^2 carbon layer. The most intensely populated nuclei were ^{165,166,167}Tm [18–20], ^{165,166}Er [18,19], and ^{163}Ho [21] corresponding to the 6n, 5n, 4n, 5np, 4np, and $\alpha 4n$ channels, respectively. The γ rays emitted by the evaporation residues were detected using the GASP array [22], consisting of 40 Compton suppressed large volume Ge detectors, and a multiplicity filter of 80 BGO elements, providing the sum energy and γ-ray multiplicity used to select the different reaction channels. Events were collected when at least three suppressed Ge and three inner multiplicity filter detectors were fired. With this condition a total of 10^9 events was recorded. The data corresponding to Ge energies were sorted into fully symmetrized matrices and cubes with a variety of conditions on time, detector position, multiplicity, and sum energy of the BGO filter. In order to determine multipolarities and mixing ratios for the γ

transitions, the data were sorted to allow a directional correlation orientation (DCO) analysis. For this purpose a non-symmetrized matrix using the detectors at $\theta_2 = 90°$ with respect to the beam direction against those at $\theta_1 = 31.7°$, $36°$, $144°$, and $148.3°$ was constructed. In the GASP geometry, setting gates on stretched quadrupole transitions leads to theoretical DCO ratios $I\gamma_{\text{gate}=\theta_2}(\theta_1)/I\gamma_{\text{gate}=\theta_1}(\theta_2) \approx 1$ for stretched quadrupole transitions and ≈ 0.6 for pure stretched dipole ones (taking into account the loss of the state alignment).

Another experiment was performed at the TANDAR Laboratory in Buenos Aires, to measure half-lives of isomeric states in the range of 10–100 ns. In this experiment ^{166}Tm was populated through the ^{164}Dy(^{6}Li,$4n$) fusion-evaporation reaction at $E(^6\text{Li}) = 38$ MeV. The target consisted of a 1.5 mg/cm^2 isotopically enriched ^{164}Dy foil with a Bi backing of a thickness of 2 mg/cm^2. The experimental setup consisted of a high resolution Ge planar detector and an 11 NaI(Tl) element multiplicity filter. An E_γ-t matrix was constructed, where the time was measured relative to the multiplicity filter acting as stop in the coincidences.

B. Level scheme of ^{166}Tm

The level scheme of ^{166}Tm constructed in the present work is shown in Fig. 1 (parts A–C). Ten rotational bands composed of two signature partners plus a single signature sequence were observed. The low-spin part of the level scheme is essentially in very good agreement with previous works [12,17]. Here we extended the rotational bands to higher spins, and found interlinking transitions among them which established relative bandhead energies. The proposed spin and parity assignments to levels were partially determined by the presence of connections among the bands, the DCO ratios and total internal conversion coefficients extracted for some of these connections, and data from previous works [12,17]. Systematic comparisons with neighboring nuclei, namely, ^{162,164}Tm [8,9], and arguments based on band configurations have also been used in the spin and parity assignments. The bands have been labeled 1–11 following the order as they are drawn in Fig. 1 (parts A–C). Four bands (1–4), the ones corresponding to high-K structures, populate the $K^\pi = 6^- T_{1/2} = 340$ ms isomeric state [17] (Fig. 1, part A). The rest of the bands (5–7,9–11), those of low-K structures, and band 8 are mainly linked among them. The links between bands 4 and 5 establish the connection between the low-K and high-K structures. To show these linkings, band 4 is also plotted in Fig. 1, part B. Band 7 is plotted in parts B and C of Fig. 1 to show its linkings with bands 5 and 6 and with bands 8–10, respectively. In part C some states of bands 5 and 6 are shown to indicate the decays of bands 9 and 11, respectively.

Transition energies, spin assignments, γ-ray intensities, and DCO ratios are reported in Table I. Gamma-ray intensities were obtained from the total coincidence projection and from individual spectra in coincidence with low spin transitions and were normalized to the 151.6 keV line of band 5. Table II reports total internal conversion coefficients (extracted from intensity balances evaluated in double gated

spectra) for some low-energy transitions of special interest in the level scheme, the experimental values are compared with the theoretical ones for different electromagnetic characters [23].

In the remainder of this section a description of the level scheme is reported. Band 4 was extended at low and high spin with respect to previous work [12]. In the low part, the crossover transition of 126.5 (86.7+39.9) keV was observed in coincidence with members of band 4 (Fig. 2) and also with the 62.2 keV line. From intensity balance with the lower members of band 4, we assigned $E1$ character to the 62.2 keV out of band line, in agreement with results of the conversion electron measurement reported in Ref. [12]. Then, considering $E1$ character for the 62.2 keV transition, the total internal conversion coefficient extracted for the 39.9 keV transition is consistent with an $M1(E2)$ character (in-band transition), and the upper limit obtained for the 102.1 keV transition confirms the $E1$ character of this line (Table II). In addition, the branching ratio measured between the 126.5 and 86.7 keV produces a $B(M1)/B(E2)$ value which follows the trend of the band. The above arguments support the placement of the 126.5 and 39.9 keV transitions in the lower part of band 4. With the addition of the corresponding level to band 4, which we assigned as the (6^+) bandhead of the $\pi 7/2^+[404] \otimes \nu i_{13/2}(5/2^+[642])K^\pi = 6^+$ structure (see discussion below), spins were increased in one unit with respect to the previous work of Mannanal *et al.* [12]. Between spins $12\hbar$ and $17\hbar$, the states of bands 4 and 5 are strongly connected by stretched $E2$ and $M1(E2)$ transitions. The DCO ratios measured for some of these connections support their assigned character (see Table I), and in this way, spins and parity of band 5 are fixed without ambiguity relative to band 4. The present spin assignment of band 5 increased also in one unit the spin values reported in Ref. [12]. Band 5 has been identified as the ground state band on the basis of its assigned configuration (see Ref. [12] and the discussion below). As mentioned in the Introduction, the ground state of ^{166}Tm has been identified as the 2^+ member of the $\pi 1/2^+[411] \otimes \nu i_{13/2}(5/2^+[642])$ structure [13–16]. With our spin assignment the lower observed level of band 5 has $I^\pi = (3^+)$ and considering the ground state to be 2^+, the transition $(4^+) \rightarrow (2^+)$ is missing. We expect for this transition an energy close to 50 keV on the basis of similarities with the ^{164}Tm case [9]. In their work Mannanal *et al.* [12] reported the observation of a 57.5 keV γ ray in coincidence with lines of band 5, which can be a candidate for the $(4^+) \rightarrow (2^+)$ transition. Possibly, we could not observe this transition because it was embedded in the $K_{\alpha_{2,1}}$ (49.8 and 50.7 keV) or $K_{\beta_{1,2}}$ (57.5, 59.1 keV) Tm x rays, and/or it is highly converted. Examples of double gated coincidence spectra on lines of bands 4 and 5 are shown in Fig. 3. States of equal spin along bands 4 and 5 are close to each other with a minimum energy difference of 10 keV at $15\hbar$. Consequently, around this spin value, it is expected a strong mixing between the states. Above spin $15\hbar$ two $\alpha = 1$ sequences composed of $E2$ lines of approximately the same energy and intensity are in coincidence with the lower transitions of the $\alpha = 1$ component of bands 4 and 5. In Fig. 3(b) the 520.8,
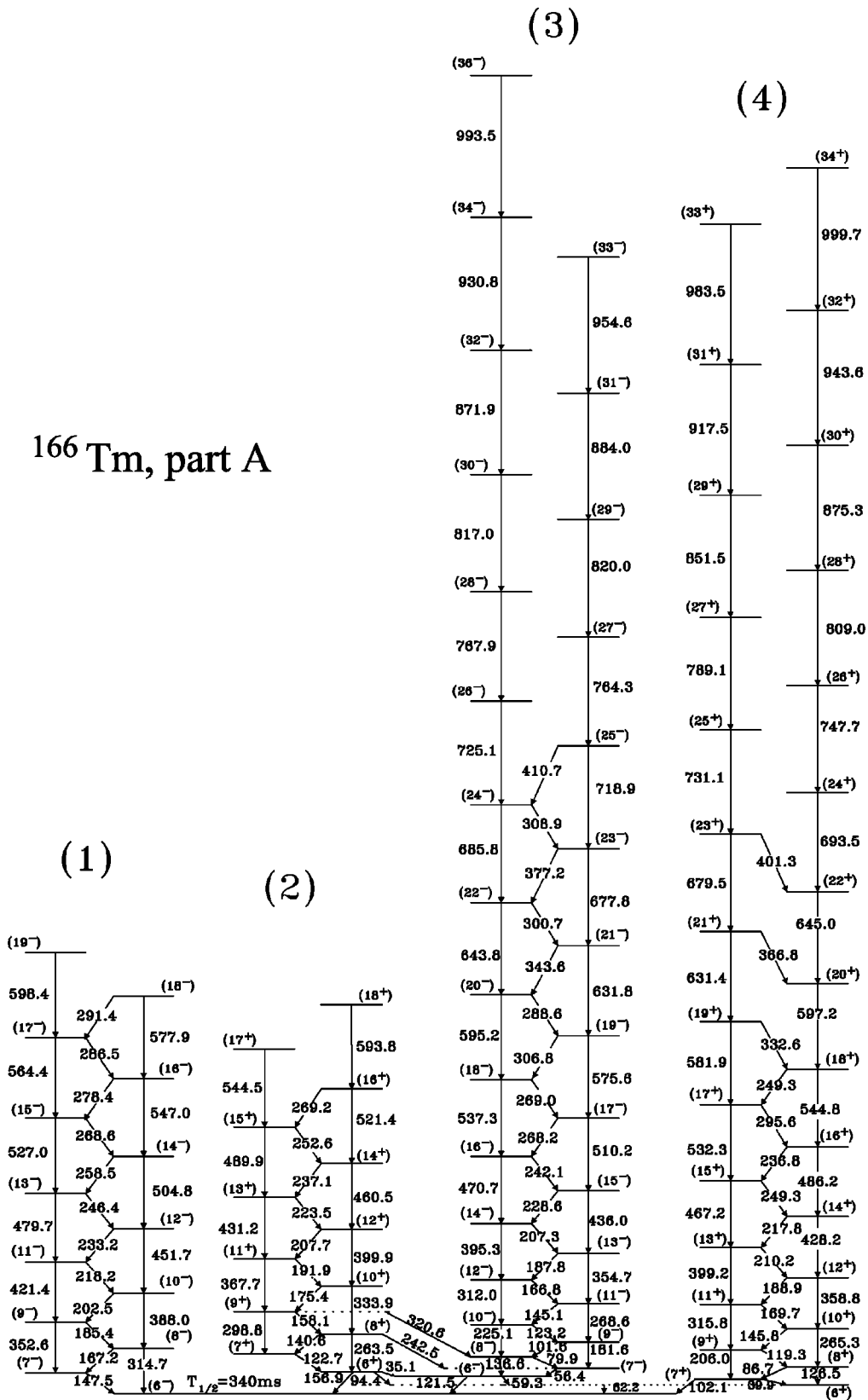
FIG. 1. Level scheme of [166]Tm divided into parts A, B, and C. The half-life of the (6[-]) isomer has been extracted from Ref. [17].
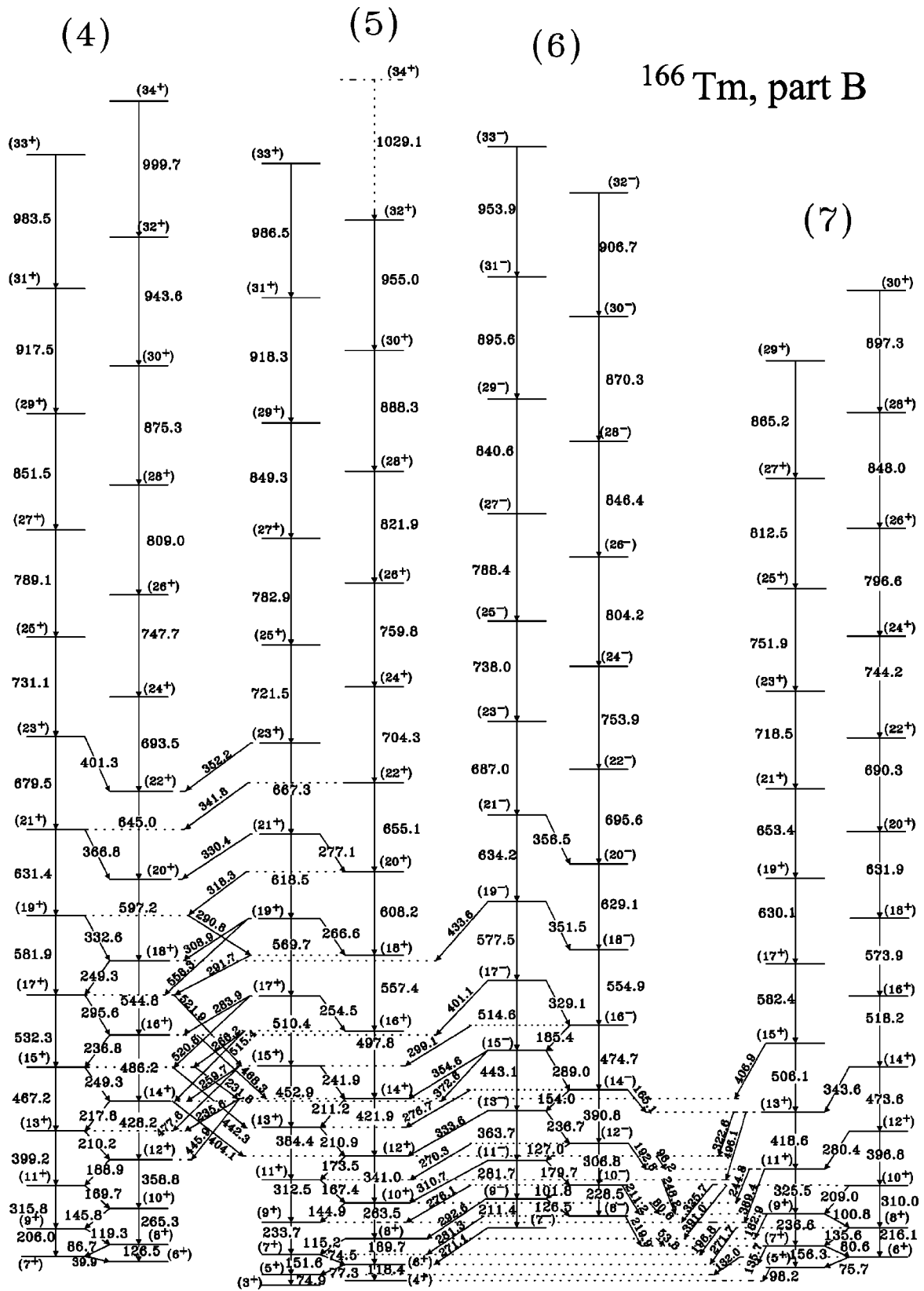
(4)

(5)

(6)

^{166}Tm, part B

(7)

FIG. 1. (*Continued.*)

FIG. 1. (*Continued.*)

569.7, 618.5, 667.3 keV, etc. lines belonging to one sequence and the 532.3, 581.9, 631.4, 679.5 keV, etc., lines belonging to the other are clearly observed, while in Fig. 3(d) we can see the 510.4, 569.7, 618.5, 667.3 keV, etc., lines belonging to one sequence and the 521.9, 581.9, 631.4, 679.5 keV, etc., lines which belong to the other. In the level scheme we plotted the 532.3, 581.9, 631.4, 679.5 keV, etc., sequence as belonging to band 4, and then the 510.4, 569.7, 618.5, 667.3

keV, etc., lines were assigned to band 5. However the other case, the sequence 520.8, 569.7, 618.5, 667.3 keV, etc., inside band 4 and consequently the 521.9, 581.9, 631.4, 679.5 keV, etc., lines inside band 5 could have been chosen in the plot of the level scheme. The larger distance between $\alpha=0$ states of equal spin of bands 4 and 5 (approximately twice the observed in the $\alpha=1$ sequences) is consistent with weaker linking transitions in comparison with the intraband

TABLE I. γ-ray transition energies, spin assignments, γ-ray intensities, and DCO ratios in ^{166}Tm obtained from the reaction ^{160}Gd(^{11}B,$5n$) at 61 MeV.

E_γ (keV)[a]	$I_i^\pi \rightarrow I_f^\pi$	I_γ[b]	R_{DCO}[c]	E_γ (keV)	$I_i^\pi \rightarrow I_f^\pi$	I_γ	R_{DCO}
Band 1				79.9	$(8^-)\rightarrow(7^-)$	440	0.83 (8)
147.5	$(7^-)\rightarrow(6^-)$			101.6	$(9^-)\rightarrow(8^-)$	595	0.80 (7)
167.2	$(8^-)\rightarrow(7^-)$			123.2	$(10^-)\rightarrow(9^-)$	780	0.9 (1)
185.4	$(9^-)\rightarrow(8^-)$	55		136.6	$(8^-)\rightarrow(6^-)$	17	
202.5	$(10^-)\rightarrow(9^-)$	32		145.1	$(11^-)\rightarrow(10^-)$	690	0.79 (9)
218.2	$(11^-)\rightarrow(10^-)$	20		166.8	$(12^-)\rightarrow(11^-)$	594	0.85 (8)
233.2	$(12^-)\rightarrow(11^-)$	17		181.6	$(9^-)\rightarrow(7^-)$	73	
246.4	$(13^-)\rightarrow(12^-)$	10		187.8	$(13^-)\rightarrow(12^-)$	475	0.80 (8)
258.5	$(14^-)\rightarrow(13^-)$	7		207.3	$(14^-)\rightarrow(13^-)$	338	0.85 (7)
268.6	$(15^-)\rightarrow(14^-)$	6		225.1	$(10^-)\rightarrow(8^-)$	208	
278.4	$(16^-)\rightarrow(15^-)$			228.6	$(15^-)\rightarrow(14^-)$	266	0.80 (9)
286.5	$(17^-)\rightarrow(16^-)$			242.1	$(16^-)\rightarrow(15^-)$	190	0.77 (8)
291.4	$(18^-)\rightarrow(17^-)$			268.2	$(17^-)\rightarrow(16^-)$	116	0.91 (8)
314.7	$(8^-)\rightarrow(6^-)$			268.6	$(11^-)\rightarrow(9^-)$	288	
352.6	$(9^-)\rightarrow(7^-)$	66		269.0	$(18^-)\rightarrow(17^-)$	147	0.9 (2)
388.0	$(10^-)\rightarrow(8^-)$	72		288.6	$(20^-)\rightarrow(19^-)$	87	0.8 (2)
421.4	$(11^-)\rightarrow(9^-)$	58	1.0(1)	300.7	$(22^-)\rightarrow(21^-)$	56	0.9 (2)
451.7	$(12^-)\rightarrow(10^-)$	56		306.8	$(19^-)\rightarrow(18^-)$	103	0.76 (8)
479.7	$(13^-)\rightarrow(11^-)$	52		308.9	$(24^-)\rightarrow(23^-)$	31	
504.8	$(14^-)\rightarrow(12^-)$	54	1.1(2)	312.0	$(12^-)\rightarrow(10^-)$	463	0.99 (7)
527.0	$(15^-)\rightarrow(13^-)$	48	1.2(2)	343.6	$(21^-)\rightarrow(20^-)$	77	0.67 (18)
547.0	$(16^-)\rightarrow(14^-)$	36		354.7	$(13^-)\rightarrow(11^-)$	492	1.06 (8)
564.4	$(17^-)\rightarrow(15^-)$	32		377.2	$(23^-)\rightarrow(22^-)$	55	0.9 (2)
577.9	$(18^-)\rightarrow(16^-)$			395.3	$(14^-)\rightarrow(12^-)$	497	0.97 (6)
598.4	$(19^-)\rightarrow(17^-)$			410.7	$(25^-)\rightarrow(24^-)$	18	
Band 2				436.0	$(15^-)\rightarrow(13^-)$	434	1.01 (6)
122.7	$(7^+)\rightarrow(6^+)$	100		470.7	$(16^-)\rightarrow(14^-)$	410	0.98 (6)
140.6	$(8^+)\rightarrow(7^+)$	70	0.8(2)	510.2	$(17^-)\rightarrow(15^-)$	313	0.93 (12)
158.1	$(9^+)\rightarrow(8^+)$	51		537.3	$(18^-)\rightarrow(16^-)$	330	1.01 (7)
175.4	$(10^+)\rightarrow(9^+)$	44		575.6	$(19^-)\rightarrow(17^-)$	340	0.99 (15)
191.9	$(11^+)\rightarrow(10^+)$	38		595.2	$(20^-)\rightarrow(18^-)$	256	0.96 (9)
207.7	$(12^+)\rightarrow(11^+)$	34		631.8	$(21^-)\rightarrow(19^-)$	224	1.05 (8)
223.5	$(13^+)\rightarrow(12^+)$	22		643.8	$(22^-)\rightarrow(20^-)$	203	0.98 (8)
237.1	$(14^+)\rightarrow(13^+)$	20		677.8	$(23^-)\rightarrow(21^-)$	147	1.06 (9)
252.6	$(15^+)\rightarrow(14^+)$	11		685.8	$(24^-)\rightarrow(22^-)$	133	1.1 (1)
263.5	$(8^+)\rightarrow(6^+)$	13		718.9	$(25^-)\rightarrow(23^-)$	66	1.1 (2)
269.2	$(16^+)\rightarrow(15^+)$	9		725.1	$(26^-)\rightarrow(24^-)$	63	0.9 (2)
298.8	$(9^+)\rightarrow(7^+)$	20		764.3	$(27^-)\rightarrow(25^-)$	31	
333.9	$(10^+)\rightarrow(8^+)$	14		767.9	$(28^-)\rightarrow(26^-)$	28	1.1 (2)
367.7	$(11^+)\rightarrow(9^+)$	24		817.0	$(30^-)\rightarrow(28^-)$	13	
399.9	$(12^+)\rightarrow(10^+)$	25		820.0	$(29^-)\rightarrow(27^-)$	10	
431.2	$(13^+)\rightarrow(11^+)$	23		871.9	$(32^-)\rightarrow(30^-)$	6	
460.5	$(14^+)\rightarrow(12^+)$	23		884.0	$(31^-)\rightarrow(29^-)$	4	
489.9	$(15^+)\rightarrow(13^+)$	20		930.8	$(34^-)\rightarrow(32^-)$	2	
521.4	$(16^+)\rightarrow(14^+)$	23		954.6	$(33^-)\rightarrow(31^-)$	2	
544.5	$(17^+)\rightarrow(15^+)$	13		993.5	$(36^-)\rightarrow(34^-)$	1	
593.8	$(18^+)\rightarrow(16^+)$	10		Band 4			
Band 3				39.9	$(7^+)\rightarrow(6^+)$	250	
56.4	$(7^-)\rightarrow(6^-)$						

TABLE I. (*Continued.*)

E_γ (keV)[a]	$I_i^\pi \to I_f^\pi$	I_γ[b]	R_{DCO}[c]	E_γ (keV)[a]	$I_i^\pi \to I_f^\pi$	I_γ[b]	R_{DCO}[c]
86.7	$(8^+)\to(7^+)$	330	0.8 (1)	189.7	$(8^+)\to(6^+)$	619	0.93 (8)
119.3	$(9^+)\to(8^+)$	348	0.97 (12)	210.9	$(13^+)\to(12^+)$	40	0.6 (2)
126.5	$(8^+)\to(6^+)$	22	1.1 (2)	211.2	$(14^+)\to(13^+)$	10	
145.8	$(10^+)\to(9^+)$	250	1.06 (10)	233.7	$(9^+)\to(7^+)$	1071	1.08 (5)
169.7	$(11^+)\to(10^+)$	160	1.2 (2)	241.9	$(15^+)\to(14^+)$	12	
188.9	$(12^+)\to(11^+)$	102	1.1 (2)	254.5	$(17^+)\to(16^+)$	19	
206.0	$(9^+)\to(7^+)$	240	0.92 (17)	263.5	$(10^+)\to(8^+)$	650	0.98 (7)
210.2	$(13^+)\to(12^+)$	66	1.1 (2)	266.6	$(19^+)\to(18^+)$	9	
217.8	$(14^+)\to(13^+)$	38	1.1 (2)	277.1	$(21^+)\to(20^+)$	2	
236.8	$(16^+)\to(15^+)$	14		312.5	$(11^+)\to(9^+)$	663	1.00 (6)
249.3	$(15^+)\to(14^+)$	13		341.0	$(12^+)\to(10^+)$	611	1.04 (6)
249.3	$(18^+)\to(17^+)$	4		384.4	$(13^+)\to(11^+)$	460	1.02 (5)
265.3	$(10^+)\to(8^+)$	502	0.97 (12)	421.9	$(14^+)\to(12^+)$	436	0.98 (7)
295.6	$(17^+)\to(16^+)$	19	1.07 (8)	452.9	$(15^+)\to(13^+)$	322	1.08 (6)
315.8	$(11^+)\to(9^+)$	590	1.00 (8)	497.8	$(16^+)\to(14^+)$	312	1.04 (8)
332.6	$(19^+)\to(18^+)$	13		510.4	$(17^+)\to(15^+)$	142	0.93 (8)
358.8	$(12^+)\to(10^+)$	600	1.08 (10)	557.4	$(18^+)\to(16^+)$	223	0.97 (10)
366.8	$(21^+)\to(20^+)$	9		569.7	$(19^+)\to(17^+)$	194	1.00 (5)
399.2	$(13^+)\to(11^+)$	510	1.03 (7)	608.2	$(20^+)\to(18^+)$	164	1.1 (1)
401.3	$(23^+)\to(22^+)$	4		618.5	$(21^+)\to(19^+)$	142	1.04 (8)
428.2	$(14^+)\to(12^+)$	480	1.07 (8)	655.1	$(22^+)\to(20^+)$	100	1.0 (1)
467.2	$(15^+)\to(13^+)$	370	1.16 (14)	667.3	$(23^+)\to(21^+)$	76	1.02 (15)
486.2	$(16^+)\to(14^+)$	375	1.06 (10)	704.3	$(24^+)\to(22^+)$	56	1.1 (2)
532.3	$(17^+)\to(15^+)$	106	1.03 (8)	721.5	$(25^+)\to(23^+)$	45	0.9 (2)
544.8	$(18^+)\to(16^+)$	267	1.04 (15)	759.8	$(26^+)\to(24^+)$	25	1.0 (2)
581.9	$(19^+)\to(17^+)$	161	0.99 (8)	782.9	$(27^+)\to(25^+)$	19	
597.2	$(20^+)\to(18^+)$	208	0.93 (15)	821.9	$(28^+)\to(26^+)$	11	
631.4	$(21^+)\to(19^+)$	114	0.9 (2)	849.3	$(29^+)\to(27^+)$	10	
645.0	$(22^+)\to(20^+)$	120	0.98 (24)	888.3	$(30^+)\to(28^+)$	6	
679.5	$(23^+)\to(21^+)$	62	1.0 (2)	918.3	$(31^+)\to(29^+)$	5	
693.5	$(24^+)\to(22^+)$	64	1.0(1)	955.0	$(32^+)\to(30^+)$	3	
731.1	$(25^+)\to(23^+)$	36		986.5	$(33^+)\to(31^+)$	2	
747.7	$(26^+)\to(24^+)$	33	0.92 (15)	1029.1	$(34^+)\to(32^+)$		
789.1	$(27^+)\to(25^+)$	15		**Band 6**			
809.0	$(28^+)\to(26^+)$	15		101.8	$(10^-)\to(9^-)$	26	
851.5	$(29^+)\to(27^+)$	7		126.5	$(9^-)\to(8^-)$	22	0.5 (1)
875.3	$(30^+)\to(28^+)$	6		127.0	$(12^-)\to(11^-)$	44	0.49 (7)
917.5	$(31^+)\to(29^+)$	4		154.0	$(14^-)\to(13^-)$	29	0.67 (13)
943.6	$(32^+)\to(30^+)$	3		179.7	$(11^-)\to(10^-)$	53	0.46 (7)
983.5	$(33^+)\to(31^+)$	2		185.4	$(16^-)\to(15^-)$	12	
999.7	$(34^+)\to(32^+)$	1		211.4	$(9^-)\to(7^-)$	26	
Band 5				228.5	$(10^-)\to(8^-)$	66	1.02 (8)
74.5	$(7^+)\to(6^+)$	50		236.7	$(13^-)\to(12^-)$	78	0.56 (6)
74.9	$(5^+)\to(3^+)$	620	0.95 (7)	281.7	$(11^-)\to(9^-)$	71	
77.3	$(6^+)\to(5^+)$	410		289.0	$(15^-)\to(14^-)$	35	0.39 (7)
115.2	$(8^+)\to(7^+)$	221	0.66 (8)	306.8	$(12^-)\to(10^-)$	247	1.00 (6)
118.4	$(6^+)\to(4^+)$	520	1.0 (1)	329.1	$(17^-)\to(16^-)$	18	
144.9	$(10^+)\to(9^+)$	94	0.69 (8)	351.5	$(19^-)\to(18^-)$	10	
151.6	$(7^+)\to(5^+)$	1000	0.98 (5)	356.5	$(21^-)\to(20^-)$	4	
167.4	$(11^+)\to(10^+)$	28	0.67 (12)	363.7	$(13^-)\to(11^-)$	155	1.10 (6)
173.5	$(12^+)\to(11^+)$	24	0.5 (1)	390.8	$(14^-)\to(12^-)$	347	1.03 (5)

TABLE I. (*Continued.*)

E_γ (keV)[a]	$I_i^\pi \to I_f^\pi$	I_γ[b]	R_{DCO}[c]	E_γ (keV)[a]	$I_i^\pi \to I_f^\pi$	I_γ[b]	R_{DCO}[c]
443.1	$(15^-) \to (13^-)$	130	1.03 (5)	Band 8			
474.7	$(16^-) \to (14^-)$	253	1.00 (3)	629.4	$(23^+) \to (21^+)$	5	
514.6	$(17^-) \to (15^-)$	81	1.00 (5)	693.0	$(25^+) \to (23^+)$	6	
554.9	$(18^-) \to (16^-)$	166	1.04 (6)	745.1	$(27^+) \to (25^+)$	3	
577.5	$(19^-) \to (17^-)$	54	1.1 (1)	804.7	$(29^+) \to (27^+)$	1	
629.1	$(20^-) \to (18^-)$	86	1.01 (8)	Band 9			
634.2	$(21^-) \to (19^-)$	34	0.9 (1)	81.1	$(6^+) \to (5^+)$		
687.0	$(23^-) \to (21^-)$	16	0.9 (1)	89.6	$(7^+) \to (6^+)$		
695.6	$(22^-) \to (20^-)$	50	0.95 (1)	121.4	$(8^+) \to (7^+)$	34	
738.0	$(25^-) \to (23^-)$	6		129.5	$(9^+) \to (8^+)$	26	
753.9	$(24^-) \to (22^-)$	22	1.1 (1)	164.8	$(10^+) \to (9^+)$	26	
788.4	$(27^-) \to (25^-)$	4		166.5	$(11^+) \to (10^+)$	8	
804.2	$(26^-) \to (24^-)$	10	1.0 (1)	170.1	$(7^+) \to (5^+)$		
840.6	$(29^-) \to (27^-)$	3		206.0	$(13^+) \to (12^+)$	7	
846.4	$(28^-) \to (26^-)$	6		206.9	$(12^+) \to (11^+)$	16	
870.3	$(30^-) \to (28^-)$	3		211.1	$(8^+) \to (6^+)$	80	
895.6	$(31^-) \to (29^-)$	2		251.4	$(9^+) \to (7^+)$	58	0.9(2)
906.7	$(32^-) \to (30^-)$	1		294.5	$(10^+) \to (8^+)$	104	
953.9	$(33^-) \to (31^-)$			331.5	$(11^+) \to (9^+)$	108	1.00(8)
Band 7				373.7	$(12^+) \to (10^+)$	92	
75.7	$(6^+) \to (5^+)$			413.4	$(13^+) \to (11^+)$	123	1.07(12)
80.6	$(7^+) \to (6^+)$	52		461.9	$(14^+) \to (12^+)$	46	
100.8	$(9^+) \to (8^+)$	49	0.7 (2)	479.2	$(15^+) \to (13^+)$	105	0.98(11)
135.6	$(8^+) \to (7^+)$	64		540.7	$(17^+) \to (15^+)$	90	0.98(15)
156.3	$(7^+) \to (5^+)$	25		546.9	$(16^+) \to (14^+)$	62	
209.0	$(10^+) \to (9^+)$	84	0.3 (2)	603.7	$(18^+) \to (16^+)$	35	
216.1	$(8^+) \to (6^+)$	131	0.9 (2)	617.2	$(19^+) \to (17^+)$	21	1.0(2)
236.6	$(9^+) \to (7^+)$	170	1.0 (2)	672.3	$(20^+) \to (18^+)$	12	
280.4	$(12^+) \to (11^+)$	27	0.5 (2)	715.9	$(21^+) \to (19^+)$	7	
310.0	$(10^+) \to (8^+)$	144	1.1 (2)	749.5	$(23^+) \to (21^+)$	3	
325.5	$(11^+) \to (9^+)$	312	1.03 (8)	Band 10			
343.6	$(14^+) \to (13^+)$	8		86.8	$(8^+) \to (7^+)$	48	
396.8	$(12^+) \to (10^+)$	110	0.8(2)	120.2	$(7^+) \to (6^+)$	46	
418.6	$(13^+) \to (11^+)$	177	1.04(8)	128.7	$(10^+) \to (9^+)$	41	0.59(15)
473.6	$(14^+) \to (12^+)$	76		160.9	$(9^+) \to (8^+)$	78	0.62(20)
506.1	$(15^+) \to (13^+)$	122	0.96(10)	174.4	$(12^+) \to (11^+)$	12	
518.2	$(16^+) \to (14^+)$	25		203.8	$(11^+) \to (10^+)$	29	
582.4	$(17^+) \to (15^+)$	71	1.0 (2)	207.2	$(8^+) \to (6^+)$	30	0.9(2)
573.9	$(18^+) \to (16^+)$	81		240.4	$(13^+) \to (12^+)$	28	
630.1	$(19^+) \to (17^+)$	30	1.1 (2)	247.9	$(9^+) \to (7^+)$	48	0.9 (2)
631.9	$(20^+) \to (18^+)$	62		289.9	$(10^+) \to (8^+)$	94	1.04 (12)
653.4	$(21^+) \to (19^+)$	40	0.9 (2)	332.7	$(11^+) \to (9^+)$	88	
690.3	$(22^+) \to (20^+)$	39		377.9	$(12^+) \to (10^+)$	88	
718.5	$(23^+) \to (21^+)$	13		414.9	$(13^+) \to (11^+)$	65	
744.2	$(24^+) \to (22^+)$	14		455.6	$(14^+) \to (12^+)$	60	1.0 (2)
751.9	$(25^+) \to (23^+)$	8		503.6	$(15^+) \to (13^+)$	42	
796.6	$(26^+) \to (24^+)$	5		541.0	$(16^+) \to (14^+)$	30	
812.5	$(27^+) \to (25^+)$	4		578.3	$(17^+) \to (15^+)$	27	
848.0	$(28^+) \to (26^+)$	3		598.0	$(18^+) \to (16^+)$	77	0.9 (2)
865.2	$(29^+) \to (27^+)$	2		623.6	$(20^+) \to (18^+)$	30	1.0 (2)
897.3	$(30^+) \to (28^+)$	1		654.8	$(19^+) \to (17^+)$	7	

TABLE I. (*Continued.*)

E_γ (keV)[a]	$I_i^\pi \to I_f^\pi$	I_γ[b]	R_{DCO}[c]	E_γ (keV)[a]	$I_i^\pi \to I_f^\pi$	I_γ[b]	R_{DCO}[c]
670.4	$(21^+)\to(19^+)$	5		290.8	$(19^+)\to(18^+)$	6	
Band 11				404.1	$(14^+)\to(12^+)$	153	0.95 (8)
76.9	$(6^-)\to(5^-)$			442.3	$(15^+)\to(13^+)$	32	
86.0	$(7^-)\to(6^-)$			468.3	$(16^+)\to(14^+)$	41	1.0 (1)
98.0	$(8^-)\to(7^-)$	139	0.57 (15)	521.9	$(17^+)\to(15^+)$	129	1.00 (6)
118.2	$(9^-)\to(8^-)$	133	0.75 (12)	Transitions	from band 5	to band 4	
131.1	$(10^-)\to(9^-)$	169	0.75 (25)	235.6	$(14^+)\to(13^+)$	27	
158.1	$(11^-)\to(10^-)$	186	0.9 (2)	259.7	$(15^+)\to(14^+)$	25	0.58 (12)
168.5	$(12^-)\to(11^-)$	153	0.7 (2)	266.2	$(16^+)\to(15^+)$	18	
202.5	$(13^-)\to(12^-)$	140	0.66 (15)	283.9	$(17^+)\to(16^+)$	10	
208.6	$(14^-)\to(13^-)$	108		291.7	$(18^+)\to(17^+)$	13	
216.1	$(9^-)\to(7^-)$	17		308.9	$(19^+)\to(18^+)$	9	
248.1	$(15^-)\to(14^-)$	95		318.3	$(20^+)\to(19^+)$	11	
249.7	$(10^-)\to(8^-)$	59		330.4	$(21^+)\to(20^+)$	6	
249.8	$(16^-)\to(15^-)$	70	0.68 (15)	341.8	$(22^+)\to(21^+)$		
289.3	$(11^-)\to(9^-)$	41		352.2	$(23^+)\to(22^+)$	2	
289.6	$(17^-)\to(16^-)$	45		445.9	$(14^+)\to(12^+)$	110	1.0 (1)
290.8	$(18^-)\to(17^-)$	40		477.6	$(15^+)\to(13^+)$	23	
321.7	$(19^-)\to(18^-)$	18		515.4	$(16^+)\to(14^+)$	15	
326.8	$(12^-)\to(10^-)$	50	1.1(2)	520.8	$(17^+)\to(15^+)$	160	1.00(5)
330.1	$(20^-)\to(19^-)$	17		558.3	$(19^+)\to(17^+)$	16	
345.3	$(21^-)\to(20^-)$	8		Transitions	from band 5	to band 7	
359.0	$(22^-)\to(21^-)$	5		53.8	$(8^+)\to(7^+)$	47	
371.3	$(13^-)\to(11^-)$	73	0.96(20)	80.6	$(10^+)\to(9^+)$	59	0.54 (9)
411.3	$(14^-)\to(12^-)$	74		96.2	$(12^+)\to(11^+)$	36	0.50 (8)
456.8	$(15^-)\to(13^-)$	82		248.2	$(11^+)\to(9^+)$		
497.8	$(16^-)\to(14^-)$	70		Transitions	from band 6	to band 4	
538.5	$(17^-)\to(15^-)$	69		372.6	$(15^-)\to(14^+)$	13	
579.6	$(18^-)\to(16^-)$	71		401.1	$(17^-)\to(16^+)$	7	
612.3	$(19^-)\to(17^-)$	38		433.6	$(19^-)\to(18^+)$	2	
651.9	$(20^-)\to(18^-)$	48		Transitions	from band 6	to band 5	
675.4	$(21^-)\to(19^-)$	25		270.3	$(12^-)\to(11^+)$	104	0.69 (12)
704.2	$(22^-)\to(20^-)$	32		271.1	$(7^-)\to(6^+)$	50	0.8 (2)
721.1	$(23^-)\to(21^-)$	15		276.1	$(10^-)\to(9^+)$	187	0.58 (7)
Transition	from band 2	to band 1		276.7	$(14^-)\to(13^+)$	32	0.56 (6)
156.9	$(6^+)\to(6^-)$			281.3	$(8^-)\to(7^+)$	109	0.60 (8)
Transitions	from band 2	to band 3		292.6	$(9^-)\to(8^+)$	153	0.57 (8)
35.1	$(6^+)\to(6^-)$			310.7	$(11^-)\to(10^+)$	137	0.66 (7)
242.5	$(8^+)\to(7^-)$	9		299.1	$(16^-)\to(15^+)$	6	0.6 (2)
320.6	$(9^+)\to(8^-)$	17		333.6	$(13^-)\to(12^+)$	75	0.51 (8)
Transitions	from band 2	to band 4		354.3	$(15^-)\to(14^+)$	30	0.59 (8)
94.4	$(6^+)\to(6^+)$			Transitions	from band 6	to band 7	
Transition	from band 3	to band 1		165.1	$(14^-)\to(13^+)$	15	
121.5	$(6^-)\to(6^-)$			192.8	$(12^-)\to(11^+)$	43	0.55 (11)
Transition	from band 3	to band 4		211.2	$(10^-)\to(9^+)$	50	0.60 (12)
59.3	$(6^-)\to(6^+)$			219.9	$(8^-)\to(7^+)$	19	0.60 (15)
Transitions	from band 4	to band 1		Transitions	from band 7	to band 5	
62.2	$(6^+)\to(6^-)$	$\geqslant 1120$[d]	0.8 (1)	98.2	$(5^+)\to(4^+)$		0.7 (2)
102.1	$(7^+)\to(6^-)$	180	0.66 (8)	132.0	$(6^+)\to(5^+)$		
Transitions	from band 4	to band 5		135.7	$(7^+)\to(6^+)$	90	0.72 (8)
231.8	$(15^+)\to(14^+)$	24		182.9	$(9^+)\to(8^+)$	260	0.55 (6)

TABLE I. (*Continued.*)

E_γ (keV)[a]	$I_i^\pi \to I_f^\pi$	I_γ[b]	R_{DCO}[c]	E_γ (keV)[a]	$I_i^\pi \to I_f^\pi$	I_γ[b]	R_{DCO}[c]
196.8	$(8^+)\to(7^+)$	38		103.0	$(8^+)\to(7^+)$	22	
244.8	$(11^+)\to(10^+)$	201	0.46 (9)	145.7	$(9^+)\to(8^+)$	40	1.0 (2)
271.7	$(8^+)\to(6^+)$	45		187.4	$(11^+)\to(10^+)$	48	0.70 (15)
322.6	$(13^+)\to(12^+)$	52	0.34 (10)	222.7	$(13^+)\to(12^+)$	6	0.7 (2)
325.7	$(10^+)\to(9^+)$	7	1.2 (3)	396.9	$(13^+)\to(11^+)$	33	
389.4	$(11^+)\to(9^+)$	130	1.0 (3)	461.3	$(15^+)\to(13^+)$	15	
391.0	$(10^+)\to(8^+)$	3		478.3	$(14^+)\to(12^+)$	50	
406.9	$(15^+)\to(14^+)$	13		Transitions	from band 10	to band 7	
496.1	$(13^+)\to(11^+)$	14		267.0	$(13^+)\to(12^+)$	8	
Transitions	from band 7	to band 8		296.8	$(15^+)\to(14^+)$	10	
660.0	$(23^+)\to(21^+)$	10		335.1	$(14^+)\to(13^+)$	6	
782.7	$(25^+)\to(23^+)$	1		378.3	$(16^+)\to(15^+)$	2	
Transitions	from band 7	to band 9		481.6	$(14^+)\to(12^+)$	38	
430.9	$(14^+)\to(12^+)$	7		549.2	$(16^+)\to(14^+)$	63	
588.2	$(19^+)\to(17^+)$	34		Transitions	from band 10	to band 9	
Transitions	from band 7	to band 10		107.7	$(7^+)\to(6^+)$	34	
447.0	$(14^+)\to(12^+)$	26		143.7	$(10^+)\to(9^+)$	42	0.9 (2)
510.3	$(16^+)\to(14^+)$	71		190.4	$(12^+)\to(11^+)$	13	
Transitions	from band 8	to band 7		223.6	$(13^+)\to(12^+)$	10	
687.7	$(23^+)\to(21^+)$	14		266.1	$(9^+)\to(7^+)$	22	
Transitions	from band 8	to band 9		439.0	$(14^+)\to(12^+)$	48	
682.5	$(21^+)\to(19^+)$	6		518.7	$(16^+)\to(14^+)$		
Transitions	from band 9	to band 5		Transitions	from band 11	to band 6	
141.7	$(6^+)\to(6^+)$			214.7	$(8^-)\to(7^-)$	29	
162.9	$(8^+)\to(8^+)$	28		248.1	$(9^-)\to(8^-)$	40	
193.9	$(10^+)\to(10^+)$	10		252.9	$(10^-)\to(9^-)$		
Transitions	from band 9	to band 7		309.1	$(11^-)\to(10^-)$	9	
504.4	$(14^+)\to(12^+)$	8		Other	transitions		
659.3	$(19^+)\to(17^+)$	32	1.2 (2)	621.5		8	
745.1	$(21^+)\to(19^+)$	6		629.9		9	
Transitions	from band 9	to band 10					

[a]Uncertainties between 0.1 and 0.3 keV.

[b]Uncertainties between 10 and 50 %, depending on intensity of the lines and complexity of the corresponding spectra.

[c]Directional correlation ratio $I\gamma_{gate=\theta_2}(\theta_1)/I\gamma_{gate=\theta_1}(\theta_2)$, ($\theta_1$=31.7°, 36°, 144°, and 148.3° and θ_2=90°) determined from coincidence spectra, setting gates on stretched $E2$ transitions on both axes of the DCO matrix.

[d]The intensity loss due to the half-life has not been evaluated.

lines. In this case we followed intensity arguments to establish the $\alpha=0$ transition sequence inside each band.

The above mentioned transitions 62.2 and 102.1 keV, depopulate band 4 both feeding the same state. This state was established as (6^-) on the basis of the spin and parity of band 4, the $E1$ character of the 62.2 and 102.1 keV transitions, and the $\Delta I=1$ type of the 102.1 keV line (supported by the DCO ratio, see Table I). This (6^-) state is the long-lived isomer reported in Ref. [17]. The connections between bands 4 and 5 fix the energy of the (6^-) isomeric state at 34.6(5) keV above the (5^+) state of band 5. In Fig. 4 we show the low-energy part of bands 4 and 5 together with the (6^-) isomer and its decay. Drissi *et al.* [17] observed a 34.42 keV line with a halflife of 340(25) ms in prompt coincidence with the 74.9 keV of band 5, and assumed that it depopulated

the isomer through an unseen transition of energy $E<25$ keV. Based on energy differences, we found from our present data, an energy of 0.2 ± 0.5 keV for this intermediate transition concluding that the 34.42 keV depopulates directly the isomer, as shown in Fig. 4. Furthermore, the $E1$ multipolarity of the 34.42 keV transition established by Drissi *et al.* [17] is consistent with a $(6^-)\to(5^+)$ decay giving additional support to our present spin assignment of band 5. Assuming the isomeric (6^-) state to be fully depopulated through the 34.42 keV $E1$ transition a $B(E1,34.42\,\text{keV})=1.5(1)\times10^{-11}e^2\,\text{fm}^2$ (corrected by internal conversion) is estimated for this decay. According to the structure of initial $(K^\pi=6^-)$ and final $(K^\pi=2^+,3^+)$ levels the 34.42 keV corresponds to an $E1$ $\Delta K=3,4$ transition. The hindrance factor with respect to the Weisskopf estimate $(F_W^{E1}\approx10^{11})$ falls

TABLE II. Total internal conversion coefficients for selected low energy transitions in ^{166}Tm. The experimental values α_T^{exp} were obtained from intensity balances and the theoretical values α_T^{th} from Ref. [23].

E_γ (keV)	Placement	α_T^{exp}	α_T^{th}			assigned
			$E1$	$E2$	$M1$	multipolarity
35.1	bands 2,3	$\leqslant 3$	1.02	300	10.6	$E1$
39.9	band 4	9 (3)	0.71	160	7.2	$M1(E2)$
80.6	bands 5,7	7 (2)	0.59	7.2	5.9	$M1(E2)$
102.1	bands 4,1	$\leqslant 1.5$	0.32	2.9	3.0	$E1$

FIG. 2. Sum of γ-ray coincidence spectra obtained setting gates on pairs of transitions of band 4 (265.3 and 358.8 keV plus 265.3 and 428.2 keV). The 39.9 and 126.5 keV lines added to band 4 are clearly seen.

within the systematic for a $\Delta K = 4$ transition and not to far for the evaluated data for $\Delta K = 3$ transitions [24].

Band 3 is one of the most populated bands as it is expected from its yrast character displayed over a large spin range. Figure 5(c) shows a coincidence spectrum gated on the 123.2 and 145.1 keV lines of band 3. This band decays through the 59.3 and 121.5 keV transitions both proceeding from the bandhead which has been established as (6^-) according to the structure assigned to the band (see Refs. [11,12] and the discussion below). The time spectra of the 59.3, 62.2, and 121.5 keV transitions are shown in Fig. 6. From the fits of these spectra a value of $T_{1/2} = 36(2)$ ns was adopted for the bandhead of band 3. This result differs from the 2(1) μs value reported in Ref. [17]. The isomeric character of the bandhead of band 3 is responsible for the intensity unbalance between transitions feeding and depopulating this isomer registered in the coincidence experiment due to the thin target which let the recoil nuclei to escape. The 59.3 keV transition links the bandheads of bands 3 and 4 and according to the configuration assigned to these bands has $\Delta K = 0$. The $B(E1, 59.3 \text{ keV}) = 3.3(3) \times 10^{-5} e^2$ fm^2 corresponds to a hindrance factor with respect to the Weisskopf estimate ($F_W^{E1} \approx 6 \times 10^4$) which falls within the systematic for a $\Delta K = 0$ transition [24].

Band 2 is a weakly populated band, several transitions were observed linking band 2 to bands 3, 4 and to the (6^-)340 ms isomer. The $E1$ character of the 35.1 keV line (Table II), together with the presence of the other decay-out transitions of energies 94.4, 156.9, 242.5, and 320.6 keV establish the spins and parity of band 2 and its position into the level scheme. A representative double-gated spectrum for this band is shown in Fig. 5(b).

Band 1 was placed on the (6^-)340 ms isomer on the basis of its assigned structure (see below) in agreement with Ref. [17]. No interlinking line with other bands was found. An example of a double gated for spectrum this band is shown in Fig. 5(a). Comparing Figs. 5(a) and 5(c) the different intensity between bands 1 and 3 is evident, which indicates the immediately departure of band 1 from the yrast line with increasing spin.

Band 6 was extended at high spins compared to the previous work [12]. Representative double gated spectra on $E2$ transitions belonging to the $\alpha = 0$ and $\alpha = 1$ signature components of this band are shown in Figs. 7(a) and 7(b), respectively. This band decays into band 5 through a series of transitions of energy around 300 keV. The DCO ratios obtained
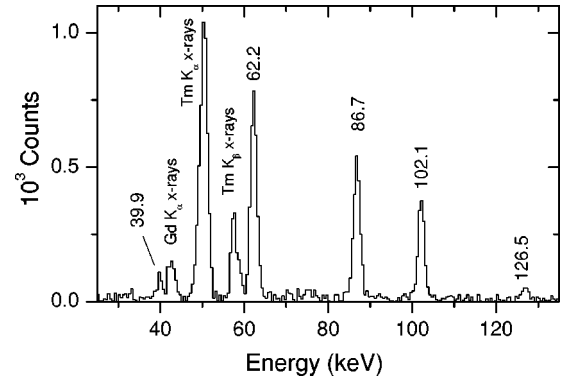
for these transitions are around 0.6 (see Table I), which require pure stretched dipole assignments. The apparent absence of quadrupole admixtures is consistent with the $E1$ and $\Delta I = 1$ assignment for each of these transitions. As an example Fig. 8(a) shows the calculated DCO ratio as a function of arctan(δ) and the experimental value for the linking 292.6 keV transition which is consistent with $-0.1 \leqslant \delta \leqslant 0.1$. As a consequence band 6 is proposed to have negative parity, if positive parity is assigned to band 5. At spin (15^-), (17^-), (19^-) this band also decays into band 4 through the lines 372.6, 401.1, and 433.6 keV, the first two ones are indicated in Fig. 3(a). This fact could be a consequence of the mixed structure of states in bands 4 and 5. Band 6 also decays into band 7 through the 165.1, 192.8, 211.2, and 219.9 keV transitions. Figures 9(a) and 9(b) show double gated coincidence spectra on pairs of lines belonging to the $\alpha = 0$ and $\alpha = 1$ components of band 7, respectively. Spins and positive parity of band 7 have been assigned from the analysis of its linking transitions mainly with band 5. For example, the total electron conversion coefficient of the 80.6 keV transition (from band 5 to band 7) corresponds to an $M1(E2)$ character (see Table II) while its DCO ratio is consistent with a $\Delta I = 1$ transition. In addition, among the strongest lines which depopulate band 7 into band 5, the 182.9, 244.8, and 322.6 keV lines present DCO ratios which are consistent with $\Delta I = 1$ $M1(E2)$ transitions with mixing ratios $\delta \leqslant 0$. In Fig. 8(b) the experimental and calculated DCO ratios for the 322.6 keV transition are shown, from this figure $-5.0 \leqslant \delta \leqslant -0.18$ was evaluated for this line. Furthermore, the DCO values of the 192.8, 211.2, and 219.9 keV transitions (see Table I), which are consistent with $\Delta I = 1$ $E1$ character, solidified our spin and parity assignments.

Around spins 12–16 $\hbar$ the $\alpha = 0$ component of band 7 is strongly linked to the $\alpha = 0$ sequences of bands 9 and 10 through transitions of energy in the range 400–550 keV, while weaker lines connect it with the $\alpha = 1$ sequence of band 10. In Fig. 9(a) these two pairs of interband lines are indicated, for example the 481.6 and 504.4 keV and the 267.0 and 296.8 keV transitions. The $\alpha = 1$ component of band 7 interacts strongly with the $\alpha = 1$ sequence of band 9 around spins 17–19 $\hbar$, the 659.3 keV interband line is indi-
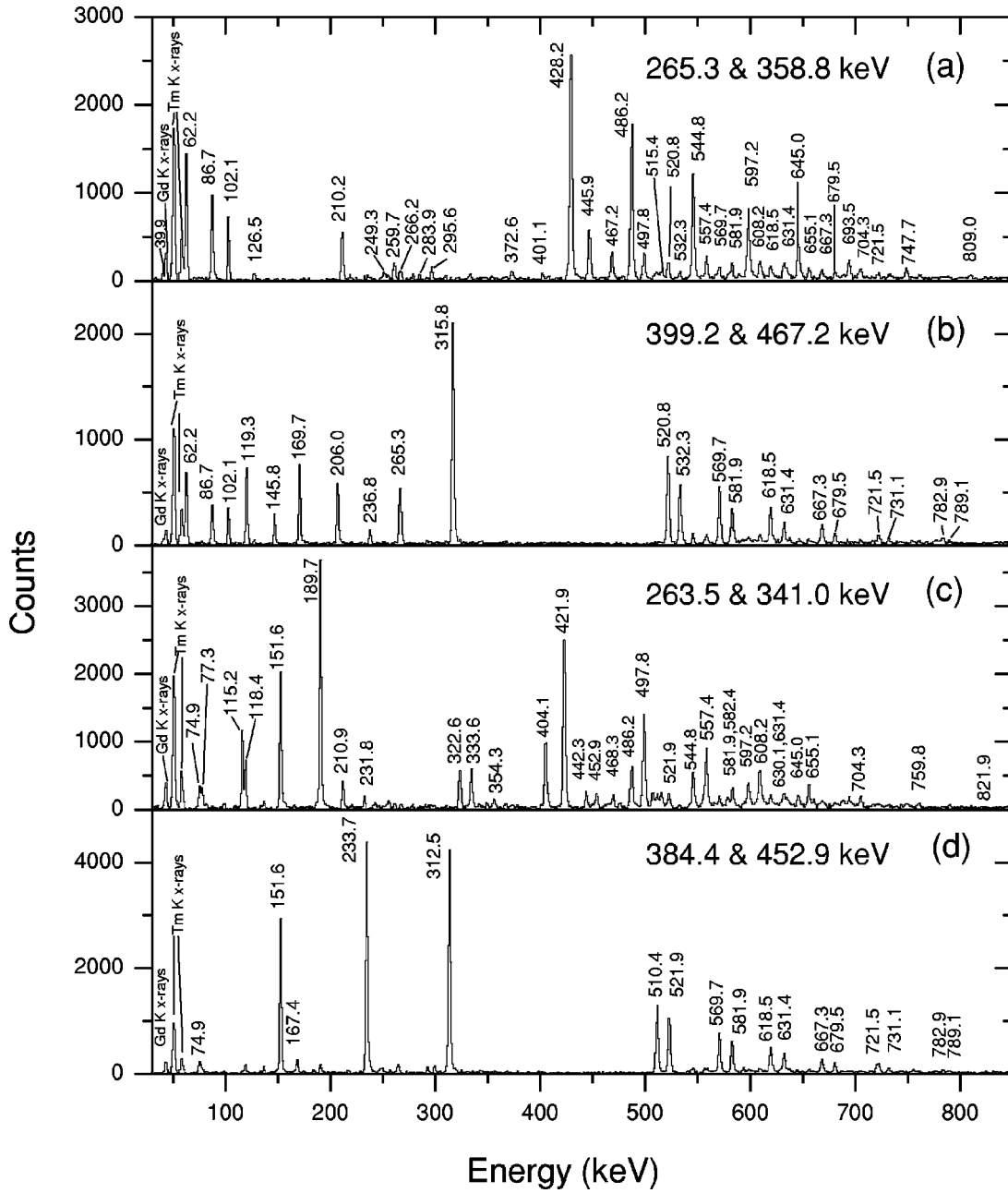
FIG. 3. γ-ray coincidence spectra of Ge detectors setting double gates on transitions of the (a) $\alpha = 0$ sequence of band 4 (265.3 and 358.8 keV), (b) $\alpha = 1$ sequence of band 4 (399.2 and 467.2 keV), (c) $\alpha = 0$ sequence of band 5 (263.5 and 341.0 keV), and (d) $\alpha = 1$ sequence of band 5 (384.4 and 452.9 keV).

cated in Fig. 9(b). On the basis of the interlinking transitions among bands 7, 9, and 10, spins and parities were assigned to the two latter bands relative to band 7. The small distance of levels of equal spin in the $\alpha = 0$ components of the three bands which achieves its minimum at spin $14\hbar$, explains the presence of the connections as a consequence of strong mixing among the different band configurations. An example of this effect can be observed in Fig. 10(a), where the intraband 461.9 keV and the interband 439.0 keV transitions show approximately the same intensity. An $E2$ sequence indicated in the level scheme as band 8 has been observed linked to the $\alpha = 1$ component of bands 7 and 9. The decay of band 9 into band 5 has been observed through the 141.7, 162.6, and

193.9 keV lines which, according to our present spin and parity assignment, are $\Delta I = 0$ $M1(E2)$ transitions, being the intensity balance for these lines consistent with their expected electromagnetic character. In Fig. 10(a), which corresponds to a double gate on the 294.5 and 373.7 keV lines, the coincidences with the lower members of band 5 (151.6 and 189.7 keV lines) and with the 162.6 keV out-of-band line are clearly observed.

Finally, in the analysis of double gated spectra on pairs of transitions of band 11 we observed systematically the presence of the lower members of band 5 (namely, the 151.6 keV line) through rather weak coincidences, as is indicated in Fig. 10(e). Due to complex and low intensity coincidence rela-
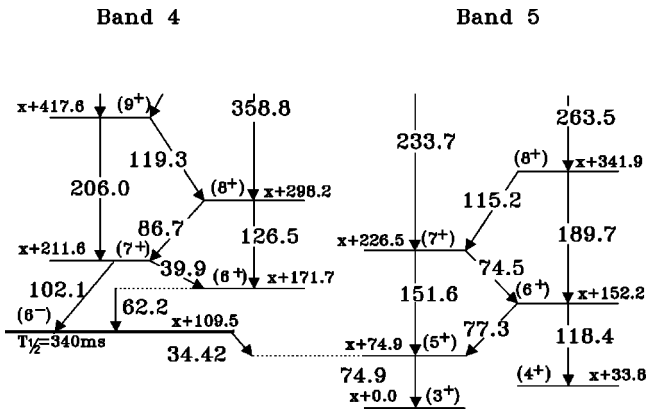
Band 4 **Band 5**

FIG. 4. Low-energy part of bands 4 and 5 and the (6^-) isomer. The energy of the transition from the level at $x+109.5$ keV to the level at $x+74.9$ keV and the half-life of the isomer have been extracted from Ref. [17].

tionships, some of the decay-out transitions were not placed into the level scheme. However, clear coincidences were observed between the members of the following pairs: 214.7 and 271.1, 248.1 and 281.3, 252.9 and 292.6, and 309.1 and 276.1 keV lines. It can be noted that for each pair the second line corresponds to an $E1$ decay transition from band 6 into band 5 (Fig. 1, part B). This fact allowed the placement of band 11. We adopted $I \rightarrow I-1$ for the decay lines from band 11 into band 6. The possibility of $I \rightarrow I-2\,E2$ transitions for these decays was discarded. In this last scenario spins of band 11 should be increased in one unit with respect to our present assignment and as a consequence, states of the same spin in bands 6 and 11 would lie very close [as an example it can be seen that the (9^-) state of band 6 and the (8^-) state of band 11 are only 3 keV apart] and strong linkings between the bands in both directions should have been observed. However, only weak connections were detected and only from band 11 to band 6. Positive parity for band 11 can not be discarded on the basis of the coincidence data analysis and to assign negative parity we invoke structure arguments, namely, the $B(M1)/B(E2)$ values, and systematic comparison with a similar structure reported in ^{164}Tm [9]. On account of coincidence relationships the 86.0 and 76.9 keV lines [which are indicated in Fig. 10(e)] lie at the bottom of band 11, however, the absence of observed crossover transitions forbid an unambiguously placement of these lines. To
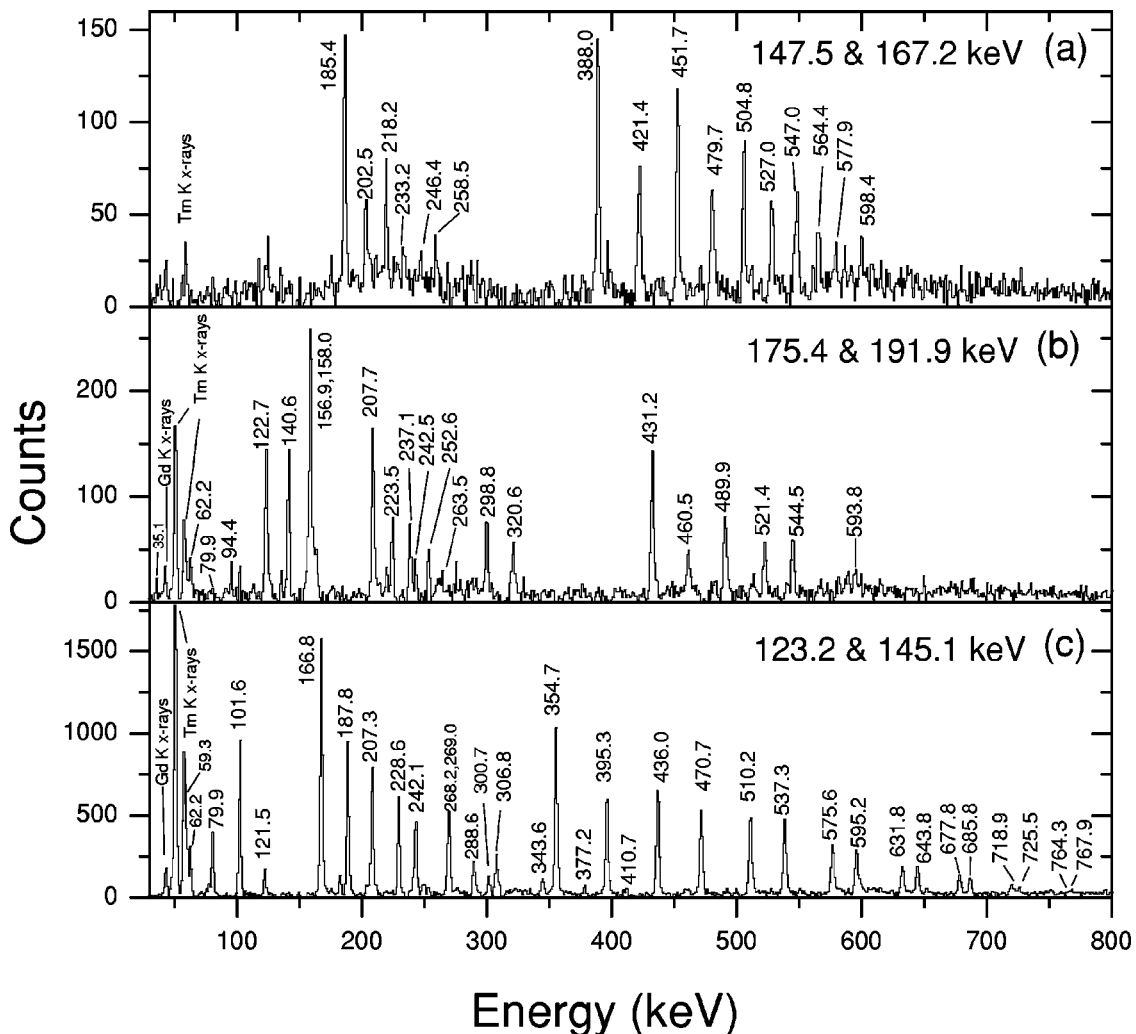

FIG. 5. Representative spectra obtained setting double gates on transitions of (a) band 1 (147.5 and 167.2 keV), (b) band 2 (175.4 and 191.9 keV), and (c) band 3 (123.2 and 145.1 keV).
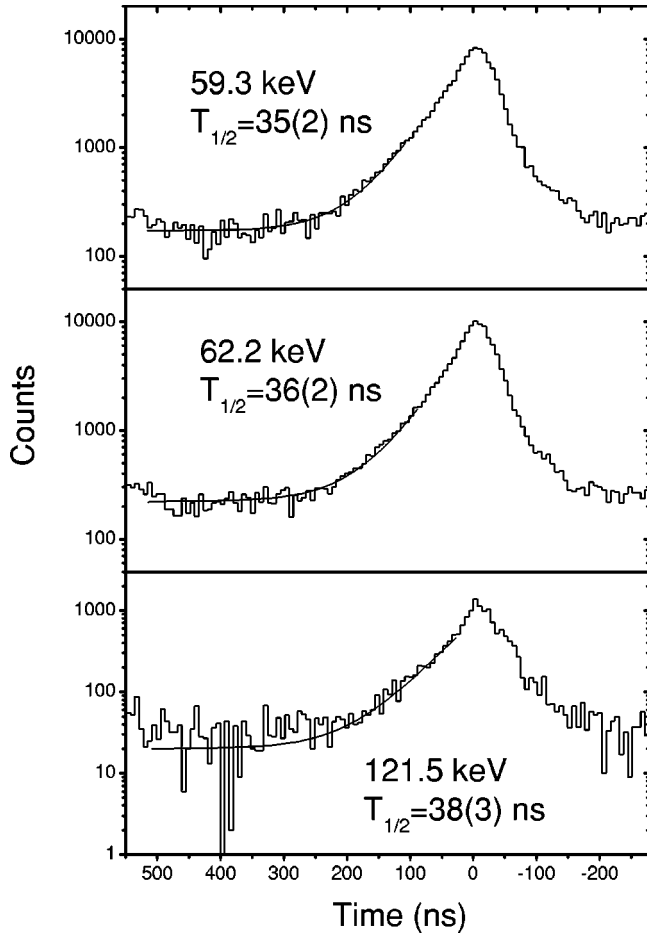
FIG. 6. Time distribution of the 59.3, 62.2, and 121.5 keV lines arising from the NaI (Tl) multiplicity filter and planar detector coincidences. The best fits through the data points are also shown.

show this fact we indicated the two lower states of band 11 with dotted lines in the level scheme. Examples of double gated coincidence spectra for bands 9–11 are shown in Fig. 10.

For coupled bands with connecting $\Delta I = 1 M1(E2)$ mixed transitions the experimental $B(M1)/B(E2)$ ratios were determined by the following expression:

$$\frac{B(M1,I \to I-1)}{B(E2,I \to I-2)} = 0.697 \frac{E_{\gamma_2}^5}{E_{\gamma_1}^3} \frac{1}{\lambda(1+\delta^2)} \left[\frac{\mu_N^2}{(e\,b)^2} \right],$$

where E_{γ_1} and E_{γ_2} are the energies (in MeV) corresponding to the $\Delta I = 1$ and $\Delta I = 2$ transitions, respectively, λ the γ-ray intensity ratio $I(\gamma_2)/I(\gamma_1)$, and δ the mixing ratio of the $\Delta I = 1$ transition. The experimental branching ratios (λ) were obtained from relative γ-ray intensities in the spectra in coincidence with transitions directly populating the corresponding states. In the evaluation of $B(M1)/B(E2)$, we assumed $\delta^2 = 0$ (in most cases the error produced with this assumption is less than 10%).

III. DISCUSSION

The bands expected at low excitation energy in ^{166}Tm are those built on the lowest proton and neutron orbitals in the neighboring odd-Z and odd-N nuclei. In order to identify these bands we studied the evolution of Nilsson levels in the vicinity of ^{166}Tm as a function of the neutron number. In Fig. 11 the bandhead energies have been plotted for the odd Yb, Tm, and Er isotopes [21,18,20,25]. For the doubly odd ^{166}Tm we constructed the zero-order level scheme [2] adding the experimental bandhead energies extracted from neighbor-
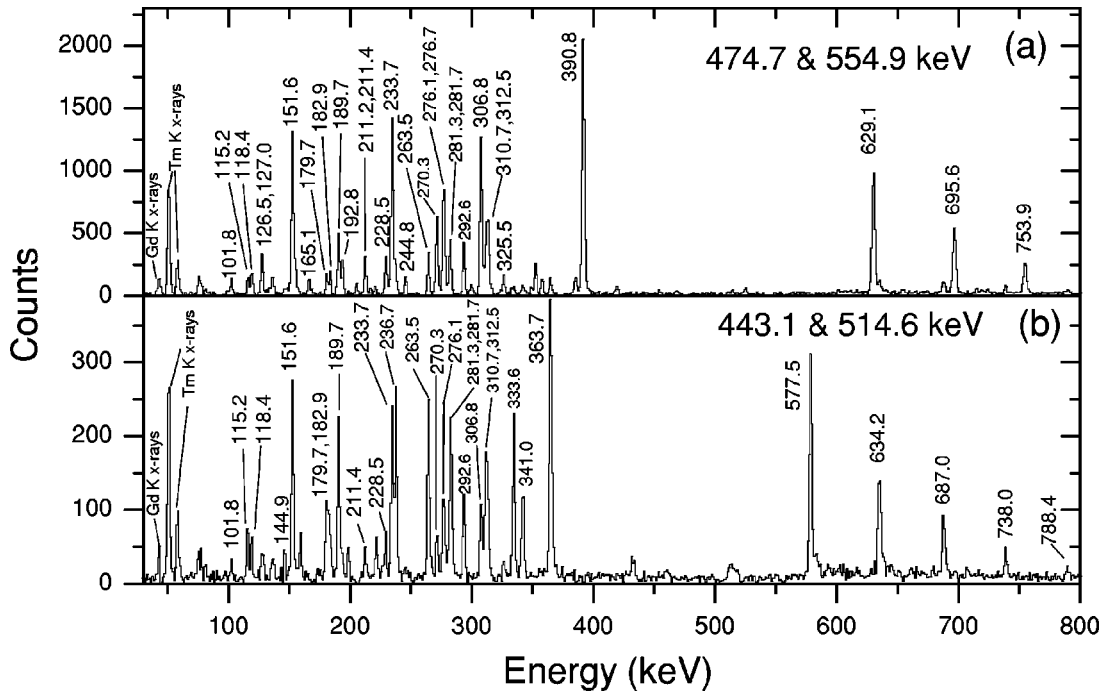

FIG. 7. Representative double gated γ-ray coincidence spectra of Ge detectors on pairs of transitions of the (a) $\alpha = 0$ sequence of band 6 (474.7 and 554.9 keV) and (b) $\alpha = 1$ sequence of band 6 (443.1 and 514.6 keV).
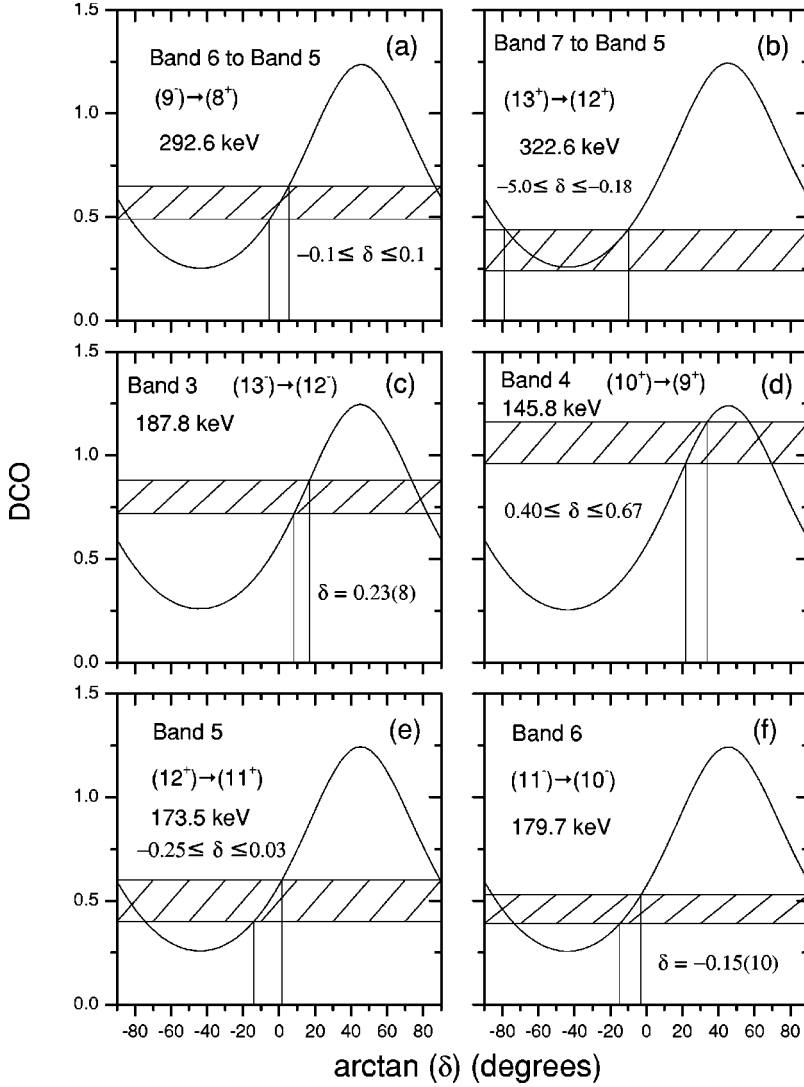
FIG. 8. Calculated DCO ratios as a function of arctan (δ) and experimental values for selected transitions (a) $(9^-)\rightarrow(8^+)$ 292.6 keV from band 6 to band 5, (b) $(13^+)\rightarrow(12^+)$ 322.6 keV from band 7 to band 5, (c) $(13^-)\rightarrow(12^-)$ 187.8 keV of band 3, (d) $(10^+)\rightarrow(9^+)$ 145.8 keV of band 4, (e) $(12^+)\rightarrow(11^+)$ 173.5 keV of band 5, (f) $(11^-)\rightarrow(10^-)$ 179.7 keV of band 6. Gating is done on stretched quadrupole transitions and a dealignment parameter $\sigma/I=0.3$ was used for the substate population distribution.

ing odd proton and odd neutron isotopes and neglecting the residual interaction which can split the $K_{\pm}=|\Omega_p\pm\Omega_n|$ states according to the Gallagher-Moszkowski coupling rules [26] (see Table III). For the ^{166}Tm rotational bands found in the present work, the configuration assignment was based on systematics and on the analysis of band properties such as rotation alignments, band crossing frequencies $B(M1)/B(E2)$ values, mixing ratios of $M1(E2)$ transitions, signature splitting, etc. The theoretical estimates of the $B(M1)/B(E2)$ were obtained from the semiclassical formula of the cranking model developed by Dönau and Frauendorf [27] (see also Ref. [28]). We used the following expressions:

$$B(E2,I\rightarrow I-2)=\frac{5}{16\pi}\langle IK20|I-2K\rangle^2 Q_0^2$$

and

$$B(M1,I\rightarrow I-1)=\frac{3}{8\pi}\mu_T^2,$$

where μ_T is the transverse magnetic moment given by

$$\mu_T=(g_{\Omega_p}-g_R)(\Omega_p\sqrt{1-K^2/I^2}-i_pK/I)+(g_{\Omega_n}-g_R)$$
$$\times(\Omega_n\sqrt{1-K^2/I^2}-i_nK/I),$$

in units of μ_N. Q_0 is the intrinsic quadrupole moment, g_{Ω_p}, g_{Ω_n}, and $g_R=0.3$ are the proton, neutron, and collective gyromagnetic factors, respectively. The quantities i_p and i_n represent the aligned angular momenta of the proton and the neutron, respectively.

The mixing ratio δ for $\Delta I=1$ in-band transitions was evaluated using the expression

$$\delta=0.93E_\gamma Q_0 K\sqrt{I^2-K^2}/(\mu_T I^2),$$

where E_γ is the transition energy in MeV, Q_0 and μ_T are in units of e b and μ_N, respectively. We used $Q_0=7.5\ e$ b, which corresponds to an average of the experimental values for the neighboring even-even Er and Yb nuclei [29]. Proton and neutron g factors (g_{Ω_p}, g_{Ω_n}) were calculated by the expression [30] $g_\Omega=g_l+(g_s-g_l)\langle s_3\rangle/\Omega$. The expectation values of the spin projection on the symmetry axis $\langle s_3\rangle$ were evaluated using Nilsson-type wave functions obtained from
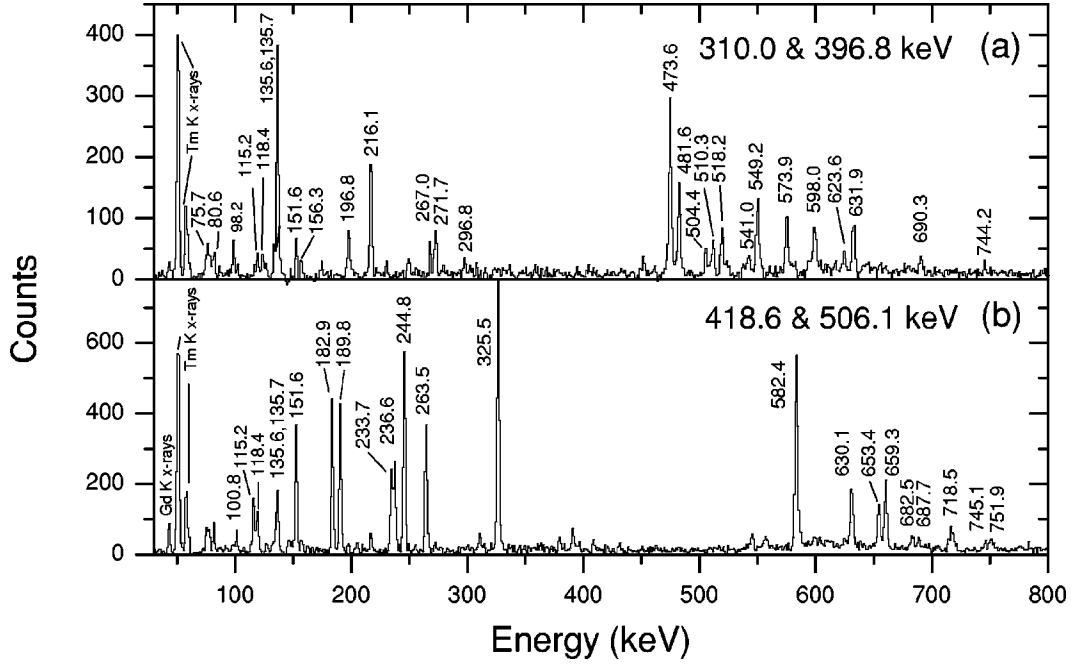
FIG. 9. γ-ray coincidence spectra of Ge detectors gated on pairs of transitions belonging to the (a) $\alpha=0$ sequence of band 7 (310.0 and 396.8 keV) and (b) $\alpha=1$ sequence of band 7 (418.6 and 506.1 keV).

the diagonalization of the deformed harmonic oscillator with $\beta=0.30$, the parameters κ and μ were extracted from Ref. [30]. For the orbital and spin g factors we used: $g_{l,p}=1$, $g_{s,p}=3.91$, $g_{l,n}=0$, and $g_{s,n}=-2.68$. Alignments and g factors for the proton and neutron intrinsic states used in the calculations are listed in Table IV. Figure 12 shows experimental and calculated $B(M1)/B(E2)$ values for bands 1–7 and 9–11. In Table III we report the sign of the mixing ratio evaluated for the $\Delta I=1$ in-band transitions of the different configurations.

A $\Delta I=2$ sequence in a rotational band can be analyzed in terms of the cranking model. The inertia parameters, J_0 and J_1 are extracted fitting the Harris expression

$$R=I_x-i=(J_0+J_1\omega^2)\omega,$$

where R is the collective and i the particle contribution (which is also set as a free parameter in the calculation) to the total aligned angular momentum $I_x(I)=\sqrt{(I+\frac{1}{2})^2-K^2}$, and K represents the projection of the angular momentum on the nuclear symmetry axis. The rotational frequencies (ω) are derived from the experimental level spacing with the usual relation [31]

$$\hbar\omega=\frac{E(I+1)-E(I-1)}{I_x(I+1)-I_x(I-1)},$$

where $E(I)$ is the energy of the level of spin I. The fitting intervals are chosen in a frequency range corresponding to fully aligned particles without breaking pair effects. The alignments listed in Table IV and the inertia parameters J_0 and J_1 used for band 6 of ^{166}Tm and for the single-nucleon components in neighboring odd-A nuclei presented below, were extracted by this procedure.

A clearest distinction among the bands is connected to the lowest observed crossing frequency. In bands containing the $\nu i_{13/2}(5/2^+[642])$ orbital, the first $i_{13/2}$ crossing (called the AB crossing) is blocked. These bands show the second $i_{13/2}$ (BC) crossing delayed ≈ 0.07 MeV with respect to the AB crossing. In order to establish crossing frequencies we studied the evolution of the dynamical moment of inertia $J^{(2)}$ along the rotational band. We used the following approximations to evaluate $J^{(2)}$ vs $\hbar\omega$:

$$J^{(2)}=\frac{dI_x}{d\omega}\simeq\frac{4\hbar^2}{E_{\gamma_2}-E_{\gamma_1}}$$

and

$$\hbar\omega=\frac{E_{\gamma_1}+E_{\gamma_2}}{4},$$

where E_{γ_1} and E_{γ_2} are the energies of two consecutive $\Delta I=2$ transitions in the rotational band. The $J^{(2)}$ parameter is very sensitive to changes in the moment of inertia caused by level crossing implying particle alignments and in this way can be used to determine crossing frequencies avoiding the difficulties of selecting reference inertia parameters. The position of peaks and/or of sudden and large variations in the plot of $J^{(2)}$ vs $\hbar\omega$ was adopted as the crossing frequency. In Fig. 13 we plotted the dynamical moments of inertia corresponding to bands of ^{166}Tm and different bands in the neighboring nuclei. The yrast band in the even-even nucleus ^{164}Er [32] represents the behavior of the even-even core and the bands in ^{167}Yb [20], ^{163}Er [21], and ^{165}Tm [33] display the effect produced by the odd particle. In the odd-odd nucleus ^{166}Tm we expect the combination of both odd particle ef-
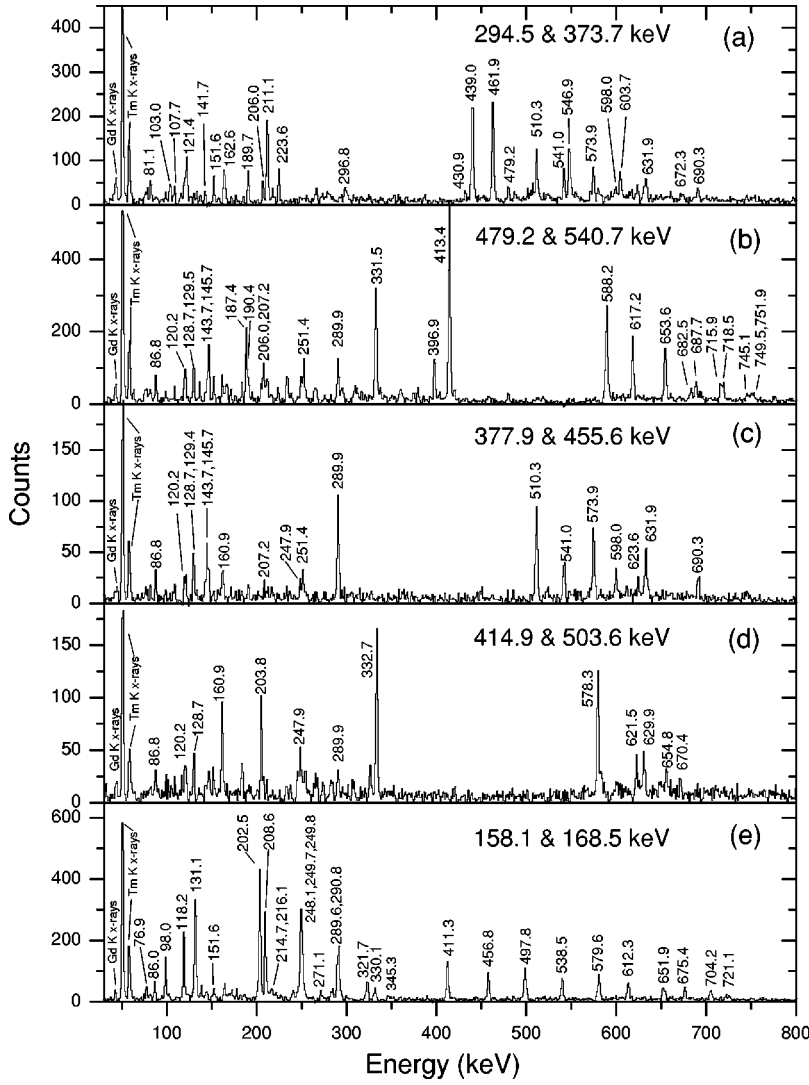
FIG. 10. Selected γ-ray coincidence spectra of Ge detectors gated on pairs of transitions of (a) band 9, $\alpha=0$ component (294.5 and 373.7 keV), (b) band 9, $\alpha=1$ component (479.2 and 540.7 keV), (c) band 10, $\alpha=0$ component (377.9 and 455.6 keV), (d) band 10, $\alpha=1$ component (414.9 and 503.6 keV), and (e) band 11 (158.1 and 168.5 keV).

fects. The crossing frequencies extracted from Fig. 13 are listed in Table V, where we also included the deviation of the crossing frequencies with respect to the even-even core ($\delta\hbar\omega_c$) and for the bands of ^{166}Tm the calculated deviations, adding the effects of the proton and neutron involved in the configuration of the band ($\delta\hbar\omega_c^{\mathrm{calc}}$), are also reported.

A. High-K structures: bands 1, 2, and 3

For band 1 we propose the configuration $\pi 7/2^+[404] \otimes \nu 5/2^-[523]K^\pi=6^-$ in agreement with Ref. [17]. This high-K normal band is consistent with its effective projection quantum number $K_{\mathrm{eff}}=6.5$. This parameter is obtained from the energy ratio of the first two $\Delta I=1$ transitions (x), according to the formula $K_{\mathrm{eff}}=(2-x)/(x-1)$, assuming a rotational band with energy states $E(I)=(\hbar^2/2J)[I(I+1) -K^2]$, as described in Ref. [2]. The high value of K_{eff} obtained for band 1 corresponds to the case in which both proton and neutron orbitals are weakly affected by the Coriolis interaction, resulting in $K_{\mathrm{eff}}\approx K=\Omega_p+\Omega_n=7/2+5/2=6$. The 6^- bandhead of this structure appears as the lowest high-K configuration predicted by the zero-order level scheme (Table III), and was identified as the 340 ms isomeric

state [17]. In Fig. 12 we compare the theoretical $B(M1)/B(E2)$ values with the experimental ones. Even taking into account the large mixing ratios of this structure ($\delta \approx 0.9$) the experimental points are rather underestimated by the calculation. The estimation of the crossing frequency, $\hbar\omega_c\approx 0.28$ MeV, obtained from the dynamical moments of inertia [Fig. 13(e) and Table V] is consistent with the first $\nu i_{13/2}$ crossing (AB).

As mentioned above, band 2 has positive parity and spins determined according to its connections with band 3, establishing a bandhead $I=6$, which is approximately equal to the extracted $K_{\mathrm{eff}}=5.9$. This is consistent with a normal band in which the $\nu i_{13/2}$ orbital is not involved. This can not be confirmed by the crossing frequency because the $\nu i_{13/2}$ crossing is not reached. We propose for band 2 the $\pi 7/2^-[523] \otimes \nu 5/2^-[523]K^\pi=6^+$ configuration which, according to the zero-order level scheme of ^{166}Tm (Table III) predicts a 6^+ bandbead energy for this structure at 227 keV. In addition, the observed $B(M1)/B(E2)$ values of band 2 are in very good agreement with this interpretation (Fig. 12).

The structure assigned to band 3 is $\pi 7/2^-[523] \otimes \nu i_{13/2}(5/2^+[642])K^\pi=6^-$ in agreement with Refs.
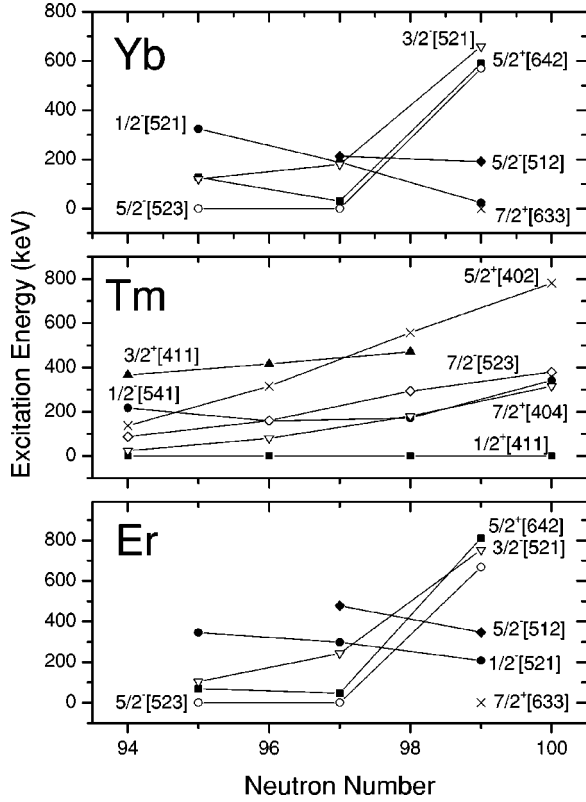
FIG. 11. Bandhead excitation energies for odd ^{165,167,169}Yb, ^{163,165,169}Tm, and ^{163,165,167}Er isotopes.

ture. However, the DCO ratios of the $\Delta I = 1$ in-band transitions indicate positive mixing ratios excluding the presence of the $\pi h_{9/2}$ orbital (Table III). An example of the DCO ratios is shown in Fig. 8(c) where a mixing ratio $\delta = 0.23(8)$ is obtained for the $(13^-) \rightarrow (12^-)$ 187.8 keV transition. The $B(M1)/B(E2)$ properties of this band are consistent with its configuration assignment (Fig. 12).

B. High-*K* structure, band 4 and low-*K* structure, band 5

The structures assigned to bands 4 and 5 are $\pi 7/2^+[404] \otimes \nu i_{13/2}(5/2^+[642])K^\pi = 6^+$ and $\pi 1/2^+[411] \otimes \nu i_{13/2}(5/2^+[642])K^\pi = 2^+, 3^+$, respectively, in agreement with Ref. [12]. In band 4, the DCO values, around $0.8-1.2$ measured for the $\Delta I = 1$ in-band transitions, are consistent with large and positive mixing ratios. This is in agreement with the proposed configuration for which a variation of δ from 0.3 up to 9 is predicted when the spin increases from 8 up to $23\hbar$. As an example, the mixing ratio of the $(10^+) \rightarrow (9^+)$ 145.8 keV transition extracted from the DCO analysis [Fig. 8(d)] is close to the calculated value ($\delta = 0.7$). The non-negligible δ values were taken into account and the quantities $B(M1)/B(E2)(1+\delta^2)$ are compared favorably with experiment (Fig. 12).

The small values of $B(M1)/B(E2) \approx 0.01 - 0.04\mu_N^2/e^2$ b^2 of band 5 are close to the expected ones for the configuration $\pi 1/2^+[411] \otimes \nu i_{13/2}(5/2^+[642])K^\pi = 2^+$ (Fig. 12). The deviation from the general trend of the experimental values above spin $I \approx 17\hbar$ corresponds to the mixing of the states of band 4 and 5, which is not included in the calculations. This strong mixing is similar to the observed between the $\pi 7/2^+[404]$ and the $\pi 1/2^+[411]$ bands in ^{165}Tm [33]. The DCO ratios for the $\Delta I = 1$ in-band transitions of band 5, which are around $0.5-0.7$ imply small mixing ratios. As an example a mixing ratio $-0.25 \leqslant \delta \leqslant 0.03$ was evaluated for the $(12^+) \rightarrow (11^+)$ 173.5 keV transition [Fig. 8(e)]. This result is in agreement with the calculations

[11,12]. The dynamical moment of inertia of this band shows a pronounced peak at 0.35 MeV [Fig. 13(e)]. This delay in the crossing frequency is consistent with the presence of the $\nu i_{13/2}$ (Table V). The same conclusion is obtained from the $K_{\text{eff}} = 1.6 \leqslant 6$ indicating a significative compression of the band. Another possibility could be the presence of the $\pi h_{9/2}$ orbital, which produces similar delay and compressed struc-

TABLE III. Zero-order level scheme of ^{166}Tm. Entries are $K_\pm = |\Omega_p \pm \Omega_n|$ values, zero-order energies in keV, and the sign of the mixing ratio δ evaluated for the $\Delta I = 1$ in-band transitions. Excitation energies correspond to the average of ^{165}Tm and ^{167}Tm for protons and to the average of ^{165}Er and ^{167}Yb for neutrons. (The values corresponding to proton and neutron intrinsic spins aligned have been underlined.)

$\pi \Omega_p^\pi [Nn_3\Lambda]$ E_π (keV)	$\nu \Omega_n^\pi [Nn_3\Lambda]$ E_ν (keV)	$\nu 5/2^-[523]$ 0	$\nu 5/2^+[642]$ 38	$\nu 3/2^-[521]$ 211	$\nu 1/2^-[521]$ 243
$\pi 1/2^+[411]$ 0		$2^-,3^-$ $\underline{0}^-$ $\delta < 0$	$2^+, 3^+$ $\underline{38}$ $\delta < 0$	$1^-, 2^-$ $\underline{211}$ $\delta < 0$	$0^-, 1^-$ $24\underline{3}$
$\pi 7/2^+[404]$ 130		$1^-,6^-$ $13\underline{0}$ $\delta > 0$	$1^+,6^+$ $\underline{168}$ $\delta > 0$	$2^-,5^-$ $\underline{341}$ $\delta > 0$	$3^-,4^-$ $37\underline{3}$ $\delta > 0$
$\pi 1/2^-[541]$ 165		$2^+,3^+$ $16\underline{5}$ $\delta < 0$	$2^-,3^-$ $\underline{203}$ $\delta < 0$	$1^+,2^+$ $\underline{376}$ $\delta < 0$	$0^+,1^+$ $40\underline{8}$
$\pi 7/2^-[523]$ 227		$1^+,6^+$ $\underline{227}$ $\delta > 0$	$1^-,6^-$ $26\underline{5}$ $\delta > 0$	$2^+,5^+$ $43\underline{8}$ $\delta > 0$	$3^+,4^+$ $\underline{470}$ $\delta > 0$

TABLE IV. Parameters used in the calculations of $B(M1)/B(E2)$ values. The alignments were extracted from ^{165}Tm and from ^{163}Er and ^{167}Yb for the proton and neutron orbitals, respectively.

Protons orbital	$i(\hbar)$	g_Ω	Neutrons orbital	$i(\hbar)$	g_Ω
$\pi 7/2^-[523]$	0.9	1.33	$\nu 5/2^-[523]$	0.5	0.250
$\pi 7/2^+[404]$	0.5	0.626	$\nu 5/2^+[642]$	3.0	-0.306
$\pi 1/2^+[411]$	0.4	-1.11	$\nu 3/2^-[521]$	0.6	-0.378
$\pi 1/2^-[541]$	1.8	0.863			

performed for this configuration which predict $\delta \approx -0.4$ and $\delta \approx -0.2$ for the $K^\pi = 2^+$ and $K^\pi = 3^+$ couplings, respectively. The dynamical moments of inertia evaluated along bands 4 and 5 show great similarities with pronounced peaks at 0.32 MeV [Fig. 13(f)]. These delays in the crossing frequency are consistent with the presence of the neutron $i_{13/2}$ (Table V).

The evolution of the level staggering of band 5 presents interesting features. On the basis of the coupling of the fa-

vored signature of both particles, we expect $\alpha^f = \alpha_p^f + \alpha_n^f = -1/2 + 1/2 = 0$ for the normal favored sequence in band 5, however, the band displays a particular behavior with two points of signature inversion and with the $\alpha = 1$ component anomalously favored over the high spin range. In Figs. 14(a) and 14(b) the energy difference $S(I) = E(I) - E(I-1) - [E(I+1) - E(I) + E(I-1) - E(I-2)]/2$ of the levels of band 5 is plotted for the two $\alpha = 1$ sequences which can be assigned to band 5, as discussed above. Even if the amplitude of the level staggering changes, both cases display the same trend. A possible explanation of the anomalous signature splitting at high spin could be the interaction between bands 4 and 5 which pushes upwards(downwards) the $\alpha = 0(1)$ states of band 5.

C. Low-K structure $\pi h_{9/2} \otimes \nu i_{13/2}$: band 6

All the properties analyzed for band 6 are consistent with the $\pi h_{9/2}(1/2^-[541]) \otimes \nu i_{13/2}(5/2^+[642])$ $K^\pi = 2^-, 3^-$ assignment. The measured $B(M1)/B(E2)$ ratios agree with the calculated ones (Fig. 12). In addition, in-band $\Delta I = 1$ transitions have DCO ratios ≈ 0.5 which are consistent with $\delta < 0$, as expected for this structure (Table III). For example,
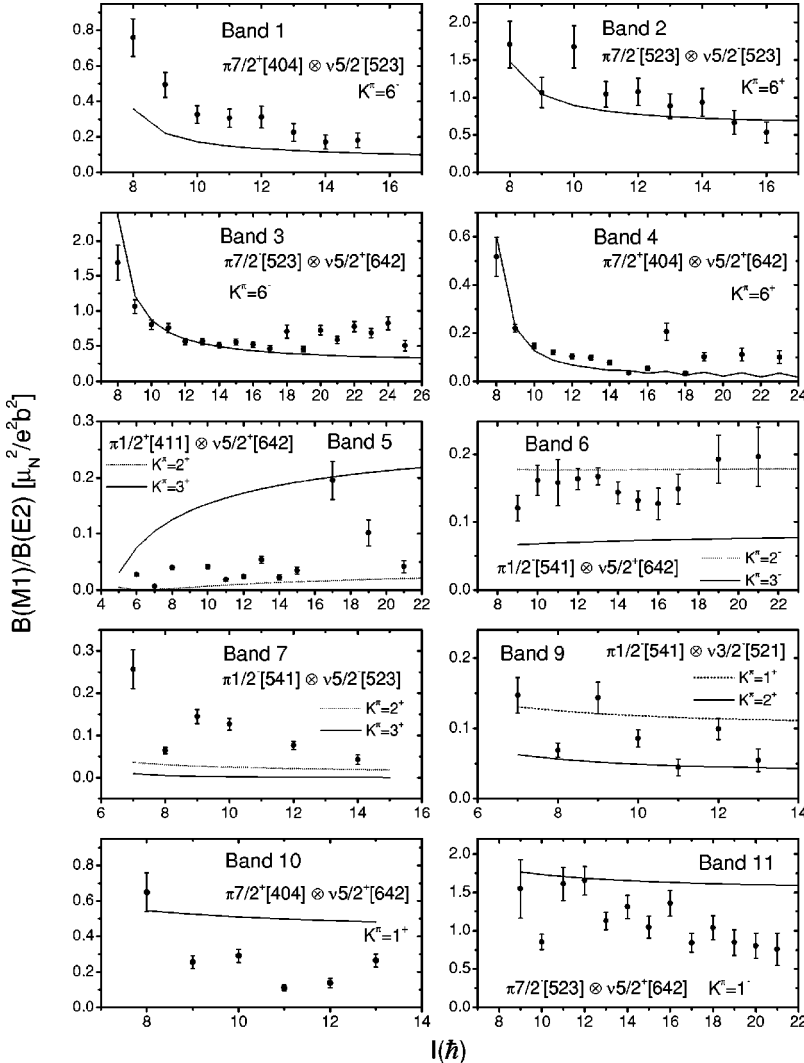

FIG. 12. Experimental $B(M1)/B(E2)$ values. The results of the calculations obtained in the framework of the cranking model for the configurations assigned are also shown. For bands 1 and 4 in which the effect of the large δ values cannot be neglected, the theoretical $B(M1)/B(E2)(1+\delta^2)$ values are plotted.
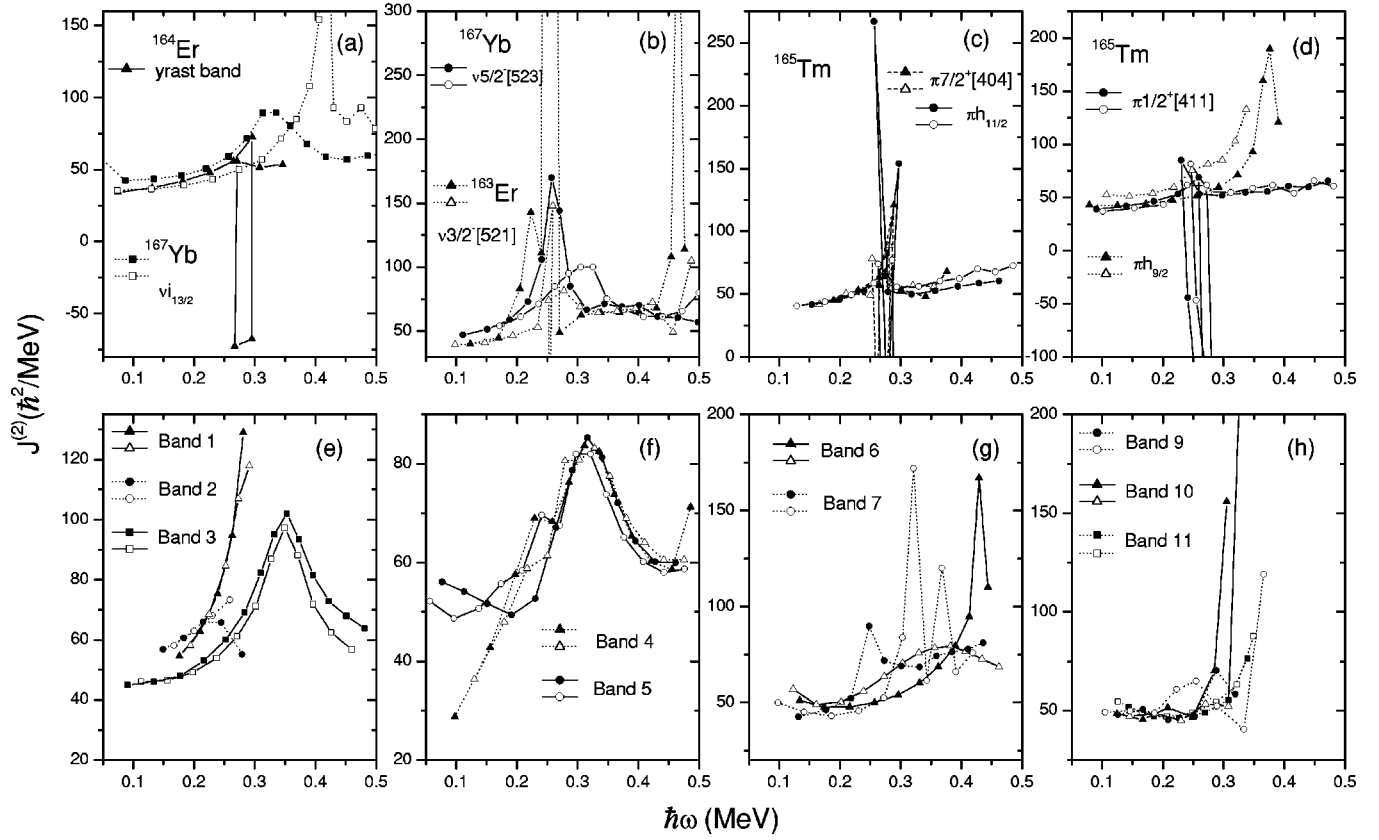
FIG. 13. Experimental dynamical moments of inertia as a function of the rotational frequency corresponding to (a) yrast band of ^{164}Er and $\nu i_{13/2}(5/2^+[642])$ band of ^{167}Yb, (b) $\nu 5/2^-[523]$ band of ^{167}Yb and $\nu 3/2^-[521]$ band of ^{163}Er, (c) $\pi 7/2^+[404]$ and $\pi h_{11/2}(7/2^-[523])$ bands of ^{165}Tm, (d) $\pi 1/2^+[411]$ and $\pi h_{9/2}(1/2^-[541])$ bands of ^{165}Tm, (e) bands 1–3 of ^{166}Tm, (f) bands 4 and 5 of ^{166}Tm, (g) bands 6 and 7 of ^{166}Tm, (h) bands 9–11 of ^{166}Tm. Filled and open circles correspond to the $\alpha=+1/2$ and $\alpha=-1/2$ signatures, respectively (odd nuclei), and $\alpha=0$ and $\alpha=1$ signatures, respectively (even-even and odd-odd nuclei).

a value of $\delta=-0.15(10)$ was extracted for the (11^-) $\rightarrow(10^-)$ 179.7 keV transition as is shown in Fig. 8(f). The alignment of the band is consistent with the sum of the $\pi h_{9/2}$ and $\nu i_{13/2}$ alignments at low spin, and it begins to upbend at considerably high frequency $\hbar\omega\approx0.4$ MeV as is shown in Fig. 15 for the $\alpha=0$ sequence. Such delayed backbend is due to the added effects of the $\pi h_{9/2}$ and $\nu i_{13/2}$ orbitals. The delay produced by the $\pi h_{9/2}$ orbital has been systematically observed in neighboring nuclei and was explained in terms of deformation changes in combination with proton-neutron interaction [9,33,34]. In addition, the evolution of the dynamical moment of inertia also reflects the delaying effects of the proton and neutron particles [Fig. 13(g) and Table V]. However, different behavior is displayed by the $\alpha=0$ and $\alpha=1$ components of the band. A pronounced peak at $\hbar\omega$ $=0.43$ MeV is observed for the $\alpha=0$ sequence while the other shows a rather smooth behavior with a maximum at $\hbar\omega\approx0.37$ MeV. Band 6 was compared with the same structures identified in ^{162,164}Tm [8,9]. In Fig. 16 the experimental Routhians are plotted for the three isotopes, using common reference parameters $(J_0=40.4\hbar^2/\text{MeV}$ and J_1 $=50.4\hbar^4/\text{MeV}^3)$. In the three cases the Routhians display similar slopes. A particular feature is observed in the three cases, the Routhians corresponding to both signatures of the band cross each other. The crossing of the signature compo-

nents can be more easily seen in a plot of the level staggering, where it appears as a reversal of the phase of the staggering. In Fig. 17 the energy difference $S(I)$ of levels of band 6 is presented together with the data corresponding to ^{162,164}Tm [8,9], the similarities displayed along the isotopic chain are evident. The point of the crossing increases with neutron number $17.3\hbar$, $19.4\hbar$, and $22.3\hbar$ for ^{162}Tm, ^{164}Tm, and ^{166}Tm, respectively. These points correspond in terms of rotational frequency to 0.29, 0.32, and 0.35 MeV, which agree within 0.01 MeV with the values extracted from the Routhian plots. It should be considered that the position of the Routhian crossing is independent of the selected reference parameters, in the case the same set is adopted for both signatures. For the present configuration the favored signature of both particles is $\alpha=+1/2$, and therefore the expected favored signature is $\alpha=1$ for the $\pi h_{9/2}\otimes\nu i_{13/2}$ band. However, at low spin the $\alpha=0$ sequence is anomalously favored up to certain point where the inversion is clearly produced. This is another example of the signature inversion phenomenon which has been extensively observed in rotational bands of odd-odd nuclei involving high-j parentage orbitals [35]. Recently, a residual proton-neutron interaction in the framework of the particle rotor model has been invoked to explain signature inversion effects in the $\pi h_{9/2}\otimes\nu i_{13/2}$ structure [6,7]. Here we employed the two-quasiparticle-plus-

TABLE V. First band-crossing frequencies and experimental and calculated deviations of these crossing frequencies with respect to the even-even core (yrast band of ^{164}Er). The calculated deviations $\delta\hbar\omega_c^{calc}$ are obtained adding the deviations of the odd-Z and odd-N neighboring nuclei.

Nucleus band	α	$\hbar\omega_c$ (MeV)	$\delta\hbar\omega_c$ (MeV)	$\delta\hbar\omega_c^{calc}$ (MeV)
^{164}Er yrast band	0	0.28		
^{165}Tm				
$\pi 7/2^-[523]$	$\pm 1/2$	0.27	-0.01	
$\pi 7/2^+[404]$	$\pm 1/2$	0.27	-0.01	
$\pi 1/2^+[411]$	$\pm 1/2$	0.26	-0.02	
$\pi 1/2^-[541]$	$+1/2$	0.38	0.10	
	$-1/2$	≥ 0.34	≥ 0.06	
^{167}Yb				
$\nu 5/2^-[523]$	$+1/2$	0.26	-0.02	
	$-1/2$	0.32	0.04	
$\nu 5/2^+[642]$	$+1/2$	0.32	0.04	
	$-1/2$	0.42	0.14	
^{163}Er				
$\nu 3/2^+[521]$	$\pm 1/2$	0.25	-0.03	
^{166}Tm				
Band 1 $\pi 7/2^+[404] \otimes \nu 5/2^-[523] K^\pi = 6^-$	0,1	≈ 0.28	≈ 0.00	-0.03
Band 2 $\pi 7/2^-[523] \otimes \nu 5/2^-[523] K^\pi = 6^+$	0,1	≥ 0.25	≥ -0.03	-0.03
Band 3 $\pi 7/2^-[523] \otimes \nu 5/2^+[642] K^\pi = 6^-$	0,1	0.35	0.07	0.03
Band 4 $\pi 7/2^+[404] \otimes \nu 5/2^+[642] K^\pi = 6^+$	0,1	0.32	0.04	0.03
Band 5 $\pi 1/2^+[411] \otimes \nu 5/2^+[642] K^\pi = 2^+,3^+$	0,1	0.32	0.04	0.02
Band 6 $\pi 1/2^-[541] \otimes \nu 5/2^+[642] K^\pi = 2^-,3^-$	0	0.43	0.15	0.24
	1	≈ 0.37	≈ 0.09	0.14
Band 7 $\pi 1/2^-[541] \otimes \nu 5/2^-[523] K^\pi = 2^+,3^+$	0	>0.43	>0.15	0.14
	1	0.32	0.04	0.08
Band 9 $\pi 1/2^-[541] \otimes \nu 3/2^-[521] K^\pi = 1^+,2^+$	0	>0.32	>0.04	0.07
	1	≥ 0.37	≥ 0.09	0.07
Band 10 $\pi 7/2^+[404] \otimes \nu 5/2^+[642] K^\pi = 1^+$	0	≥ 0.30	≥ 0.02	0.03
	1	≥ 0.33	≥ 0.05	0.03
Band 11 $\pi 7/2^-[523] \otimes \nu 5/2^+[642] K^\pi = 1^-$	0	≥ 0.34	≥ 0.06	0.03
	1	≥ 0.35	≥ 0.07	0.03

rotor calculations used many years ago to analyze a possible anomalous signature phase in the same structure in the Tl region [36], to explain the staggering of the $\pi h_{9/2} \otimes \nu i_{13/2}$ band in ^{166}Tm. The single-particle states were generated using the standard Nilsson calculation with quadrupole deformation $\beta = 0.30$ and κ and μ parameters extracted from Ref. [30]. The Nilsson Hamiltonian was diagonalized within the $N=5(6)$ shell for protons (neutrons) and the orbitals of $h_{9/2}$ ($i_{13/2}$) parentage were selected to construct the proton (neutron) particle configuration space. The pairing energy gaps ($\Delta_p = 0.83$ MeV and $\Delta_n = 0.91$ MeV) were estimated from the binding energies of the adjacent even-even and odd-A nuclei. The proton and neutron Fermi levels were positioned at 1.5 MeV below the $\pi 1/2^-[541]$ and 0.5 MeV above the $\nu 5/2^+[642]$ orbitals to reproduce the correct proton or neutron numbers, respectively. The magnitude of the $p-n$ interaction depends on the angular momentum to which the proton and neutron are coupled and on the quasiparticle character of the two valence nucleons. It was extracted from the empirical particle-hole multiplet $\pi h_{9/2} \otimes \nu^{-1} i_{13/2}$ in ^{208}Bi

[37] renormalized by pairing correlations [36]. This force has the required features to yield an intuitively transparent mechanism for signature inversion. The matrix elements $\langle (j_p j_n^{-1}) J | V_{p-n} | (j_p j_n^{-1}) J \rangle = V_J^{-1}$ display small deviations ($\sigma \approx 60$ keV) around a mean of about 150 keV for the $J = 5-10$ states while the value for $J=11$, 886 keV, is significantly larger and strongly repulsive. This means that for small collective rotation the maximally aligned state $J=9/2 + 13/2 = 11$ is excluded from the spectrum of intrinsic excitations. The system prefers to add collective angular momentum instead of aligning the particles [36]. As the system rotates faster and faster at a certain point it becomes energetically more favorable to align the two quasiparticles to $J=11$ and the change of phase of the staggering occurs. To determine the moment of inertia we kept in mind that in a real nucleus this parameter is not a constant value but usually increases with spin. A variable moment of inertia was not implemented in the calculation, so we used a fixed value and evaluated the effect of its variation on the signature inversion. An increase (decrease) in the moment of inertia causes
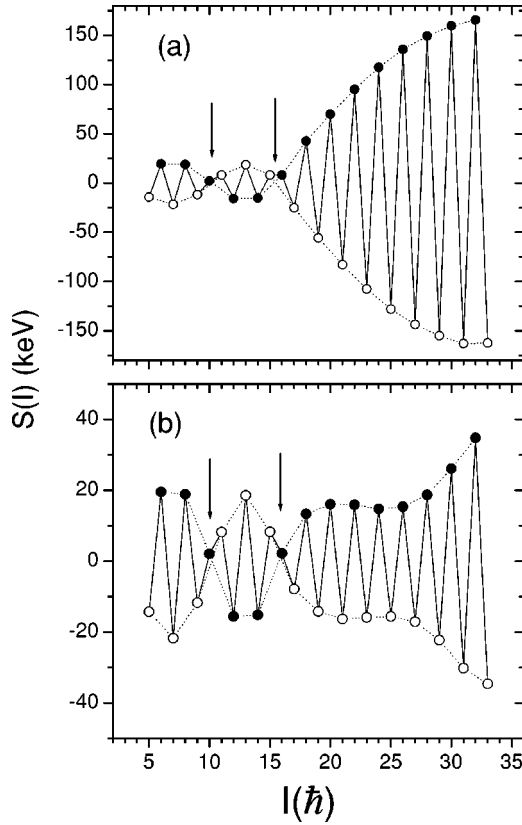
FIG. 14. Signature splitting $S(I) = E(I) - E(I-1) - [E(I+1) - E(I) + E(I-1) - E(I-2)]/2$ vs I evaluated for band 5 with the two possible $\alpha = 1$ sequences (a) 510.4, 569.7, 618.5, 667.3 keV, etc., (b) 521.9, 581.9, 631.4, 679.5 keV, etc. The arrows point to the signature inversion. Filled and open circles correspond to the $\alpha = 0$ and $\alpha = 1$ signatures, respectively.

the inversion point to move to higher (lower) spins. To present our results here, we chose a moment of inertia $J/\hbar^2 = 38.6$ MeV^{-1}. This selected value reproduces well the inversion point of band 6 and changing 8% the inertia parameter the inversion point is shifted in $\approx 1\hbar$. The results of the calculations with and without the $p-n$ force are shown in Figs. 18(a) and 18(b), respectively. Without the $p-n$ force the level staggering is determined by the Coriolis force over the entire spin range; the inclusion of the $p-n$ force reproduces the phenomenon of the low spin signature inversion and the point of the change of phase; however, the magnitude of the staggering is underestimated.

Another similarity among the isotopes ^{162,164}Tm and ^{166}Tm is observed in the decay of the $\pi h_{9/2} \otimes \nu i_{13/2}$ band into the $\pi 1/2^+[411] \otimes \nu i_{13/2}$ structure through stretched $E1$ transitions. The $B(E1)$ strength of these decays was evaluated using the following expression [33]:

$$B(E1) = 7.7 \times 10^{-3} \frac{E_{\gamma_2}^5}{E_{\gamma_1}^3} \frac{B(E2)}{\lambda} [e^2 \text{ fm}^2],$$

where E_{γ_1} and E_{γ_2} are the energies (in MeV) corresponding to the $\Delta I = 1$ interband and $\Delta I = 2$ rotational intraband tran-
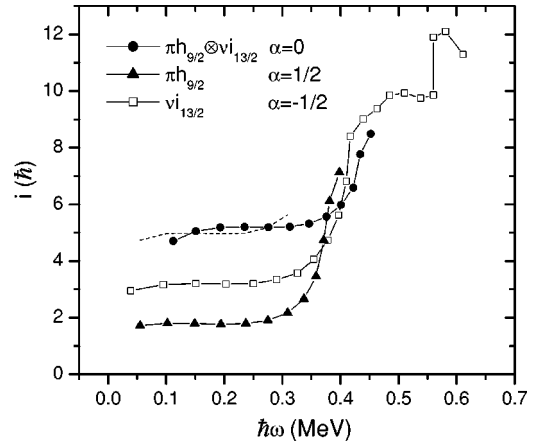

FIG. 15. Experimental alignments as a function of the rotational frequency corresponding to the $\alpha = 0$ component of the $\pi h_{9/2} \otimes \nu i_{13/2}$ band (band 6). The values for the involved single-nucleon components in neighboring odd-A nuclei, ^{165}Tm and ^{167}Yb, are also plotted, the no symbol dashed line corresponds to the sum of these values at low spin. The inertia parameters used for the reference configurations are $J_0 = 40.4\hbar^2$/MeV and $J_1 = 50.4\hbar^4$/MeV^3, $J_0 = 40.7\hbar^2$/MeV and $J_1 = 42.4\hbar^4$/MeV^3, and $J_0 = 34.9\hbar^2$/MeV and $J_1 = 54.0\hbar^4$/MeV^3 for the signature component of the $\pi h_{9/2} \otimes \nu i_{13/2}$, $\pi h_{9/2}$, and $\nu i_{13/2}$ bands, respectively.

sitions, respectively. The branching ratio λ is defined as the γ-ray intensity ratio $I(\gamma_2)/I(\gamma_1)$. $B(E2)$ is the strength of the $\Delta I = 2$ transition within the rotational band (in e^2 b^2) assumed to correspond to a quadrupole moment of 6.6, 7.1, and 7.5 e b for ^{162}Tm, ^{164}Tm, and ^{166}Tm, respectively, and evaluated using $K=2$. The quadrupole moments are the average of the experimental values for the neighboring even-even Er and Yb nuclei [29]. In Fig. 19 we compare the cor-
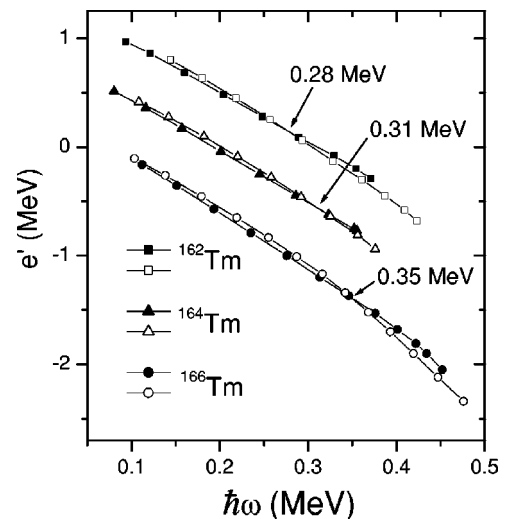

FIG. 16. Experimental Routhians versus rotational frequency for the $\pi h_{9/2} \otimes \nu i_{13/2}$ bands of ^{162,164,166}Tm. The subtracted reference has parameters $J_0 = 40.4\hbar^2$/MeV and $J_1 = 50.4\hbar^4$/MeV^3 and $K=2$ was used in the calculations. Since all the Routhians are similar in energy, those for ^{162}Tm and ^{164}Tm are shifted up in energy by 1.0 and 0.5 MeV, respectively, for the plot. Filled and open circles correspond to the $\alpha = 0$ and $\alpha = 1$ signatures, respectively.
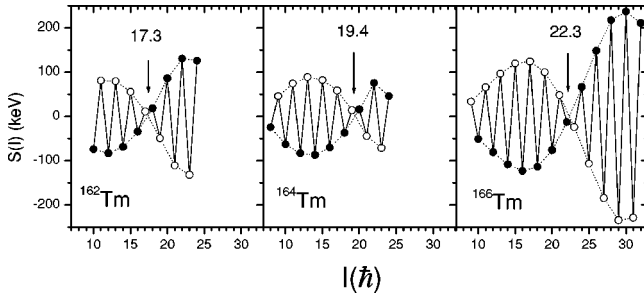
FIG. 17. Signature splitting $S(I)=E(I)-E(I-1)-[E(I+1)-E(I)+E(I-1)-E(I-2)]/2$ vs I of the $\pi h_{9/2}\otimes\nu i_{13/2}$ bands in doubly odd nuclei: ^{162,164,166}Tm. The arrows point at the signature inversion. Filled and open circles correspond to the $\alpha=0$ and $\alpha=1$ signatures, respectively.

responding $B(E1)$ strengths for the three nuclei. The order of these values is $10^{-4}-10^{-3}e^2$ fm^2, corresponding to hindrance factors relative to the Weisskopf estimate $F_W^{E1}\approx10^3-10^4$, which fall among the smaller ones displayed by the systematic [24]. In the three isotopes there is a difference in strength for the $E1$ transitions depopulating states of odd and even spins, the first ones are 1.5–4 times larger than the second ones. This signature dependence of the $B(E1)$ values was observed and discussed in Ref. [8] concerning the ^{162}Tm case. Out of band enhanced $E1$ decay modes in competition with intraband stretched $E2$ transitions have been found in a number of neighboring odd-Z nuclei, involving bands based on the $\pi1/2^+[411]$ and $\pi h_{9/2}$ structures [33,38] (the same
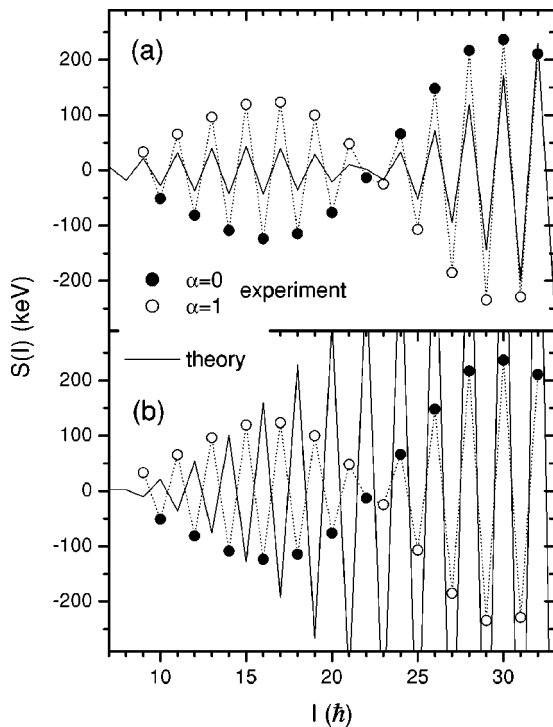

FIG. 18. Results of the two-quasiparticle-plus-rotor calculations with (a) and without (b) $p-n$ force. The experimental and calculated values $S(I)=E(I)-E(I-1)-[E(I+1)-E(I)+E(I-1)-E(I-2)]/2$ are plotted as a function of the angular momentum I.
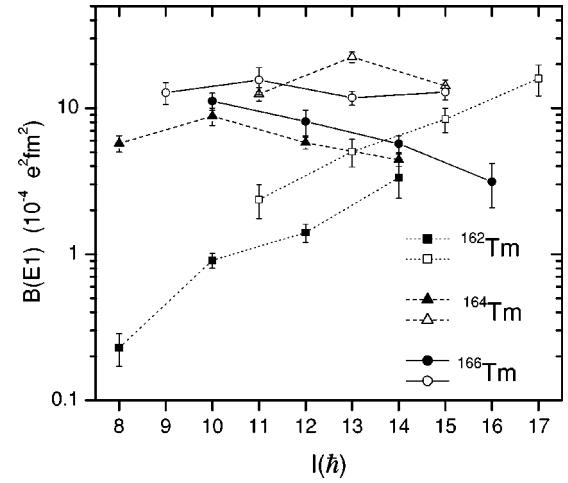

FIG. 19. Experimental $B(E1)$ values for transitions from the $\pi h_{9/2}\otimes\nu i_{13/2}$ band into the $\pi1/2^+[411]\otimes\nu i_{13/2}$ band observed in ^{162,164,166}Tm nuclei. Filled and open circles correspond to $\alpha=0\rightarrow\alpha=1$ and $\alpha=1\rightarrow\alpha=0$ transitions, respectively.

proton configurations as discussed here). The enhanced $E1$ decays have been explained in terms of coupling to octupole vibrational degrees of freedom [39,40].

D. Low-K structures: bands 7, 9–11

The $\pi h_{9/2}(1/2^-[541])\otimes\nu5/2^-[523]K^\pi=2^+,3^+$ structure was assigned to band 7, in which the favored signature of the proton is coupled to both neutron signatures. As can be seen in the level scheme (Fig. 1, part C) the $\alpha=1$ sequence of band 7 is favored over the entire band consistent with the coupling of the favored signature of both particles ($\alpha_p^f=+1/2$ and $\alpha_n^f=+1/2$). The small $B(M1)/B(E2)$ values are consistent with the proposed structure (Fig. 12). The DCO values measured for the $\Delta I=1$ in-band transitions, around ≈0.5, correspond to negative mixing ratios in agreement with the calculated values: $\delta\approx-0.4$ and $\delta\lesssim-1$ for the $K^\pi=2^+$ and $K^\pi=3^+$ couplings, respectively. Moreover, the behavior of the dynamical moment of inertia along the $\alpha=1$ component with a peak around 0.32 MeV shows the combined effects of the $\pi h_{9/2}(\alpha=+1/2)$ and the $\nu5/2^-[523](\alpha=+1/2)$ which increases and decreases the crossing frequency, respectively, with respect to the even-even core [Fig. 13(g) and Table V]. A different behavior shows the $\alpha=0$ component of band 7. The irregularities of $J^{(2)}$ around $\hbar\omega=0.25$ MeV can be associated with perturbations in the energy levels due to interactions with bands 9 and 10. Above $\hbar\omega\approx0.27$ MeV, $J^{(2)}$ remains approximately constant over the entire frequency range, which implies a large delay in the crossing frequency in agreement with the added effects of the $\pi h_{9/2}$ ($\alpha=+1/2$) and the $\nu5/2^-[523]$ ($\alpha=-1/2$) [Fig. 13(g) and Table V].

Another example of enhanced $E1$ decays in competition with $E2$ intraband transitions is observed in the decay of band 6 $\alpha=0(\alpha_p=+1/2,\alpha_n=-1/2)$ into band 7 $\alpha=1(\alpha_p=+1/2,\alpha_n=+1/2)$. In fact rather large $B(E1)$ values ($\approx10^{-3}e^2$ fm^2) were obtained for the 165.1, 192.8, and 211.2 keV decays. These $E1$ transitions can be interpreted as

a change of the neutron configuration of the states from the $\nu 5/2^+[642]$, $\alpha_n = -1/2$ to the $\nu 5/2^-[523]$, $\alpha_n = +1/2$ with the proton acting as an spectator. $E1$ decays of comparable strength have been observed in neighboring odd-N nuclei involving the $\nu 5/2^-[523]$ and the $\nu 5/2^+[642]$ structures [40,41]. For example, in ^{163}Er, $B(E1)$ values in the range, $10^{-4} - 2.5 \times 10^{-3} e^2$ fm^2, were measured for these decays and the data were favorably fitted introducing the effect of octupole vibrations on the $E1$ transition strengths [41].

The configurations assigned to bands 9 and 10 were selected among the lowest positive parity candidates presented in Table III and not identified with the previous discussed bands. We assigned the $\pi h_{9/2}(1/2^-[541]) \otimes \nu 3/2^-[521]K^\pi = 1^+, 2^+$ and the $\pi 7/2^+[404] \otimes \nu i_{13/2}(5/2^+[642])$ $K^\pi = 1^+$ configurations to bands 9 and 10, respectively. The calculated $B(M1)/B(E2)$ values fit quite well the measured ones especially for band 9 (Fig. 12). The calculations predict small mixing ratios $\delta \approx 0.04$, for the $\Delta I = 1$ transitions of the configuration of band 10 in agreement with the experimental DCO ratios around 0.6. Delaying effects in the crossing frequencies can be deduced from the evolution of the dynamical moments of inertia which are associated with the $\pi h_{9/2}$ orbital in the case of band 9 and with the blocking effect of the $\nu i_{13/2}$ orbital in the case of band 10 [Fig. 13(h) and Table V]. These delaying effects exclude the presence of the $\pi 7/2^-[523] \otimes \nu 5/2^-[523]K^\pi = 1^+$ and the $\pi 7/2^-[523] \otimes \nu 3/2^-[521]$ ($K^\pi = 2^+$ or $K^\pi = 5^+$) configurations in these bands.

Finally, we assigned the $\pi 7/2^-[523] \otimes \nu i_{13/2}(5/2^+[642])$ $K^\pi = 1^-$ configuration to band 11. A variety of arguments supports this assignment (among them, systematic comparison with ^{164}Tm [9] as mentioned above). The evolutions of the dynamical moment of inertia of band 11 [Fig. 13(h)] and band 3 [Fig. 13(e)], both involving the same proton and neu-

tron orbitals, display a similar behavior. In fact for band 3 the first maximum is produced at $\hbar\omega = 0.35$ MeV while for band 11 this maximum occurs at $\hbar\omega \geq 0.34$ MeV, as the result of the combined effects of the $\pi h_{11/2}$ and $\nu i_{13/2}$ particles in the crossing frequency (Table V). The large $B(M1)/B(E2)$ values measured for this band $\approx 1 - 2\mu_N^2/e^2\text{b}^2$ are in good agreement with the calculated ones (Fig. 12). In addition, a comparison between the low- and high-K couplings of the proton and neutron spins for the $\pi 7/2^-[523] \otimes \nu i_{13/2}(5/2^+[642])$ configuration leads to similar conclusions presented in Ref. [9], the $B(M1)/B(E2)$ ratios are $\approx 100\%$ higher for the $K = 1$ than for the $K = 6$ one.

IV. SUMMARY AND CONCLUSIONS

High-spin states in doubly odd ^{166}Tm were investigated by means of in-beam γ-ray spectroscopy techniques using the multidetector array GASP. The level scheme was extended substantially and several bands were observed at spin higher than $30\hbar$. A wealth of connections among the bands provided helpful means to assign spins and parities. Different properties of the rotational bands were analyzed leading to the identification of their structures. Signature inversion was observed in the $\pi h_{9/2} \otimes \nu i_{13/2}$ structure and this phenomenon was described by the particle rotor model calculations including an experimental $p-n$ force taken from ^{208}Bi. Pronounced $E1$ transitions were observed in the decay of the $\pi h_{9/2} \otimes \nu i_{13/2}$ band into the $\pi 1/2^+[411] \otimes \nu i_{13/2}$ and the $\pi h_{9/2} \otimes \nu 5/2^-[523]$ bands, connecting sequences of different signature. The large $B(E1)$ value of these decays is characteristic of the transitions between the $\pi h_{9/2}$ and the $\pi 1/2^+[411]$ bands and between the $\nu i_{13/2}$ and the $\nu 5/2^-[523]$ bands observed in a number of surrounding odd-Z and odd-N nuclei, respectively.

[1] A.J. Kreiner, M. Fenzl, S. Lunardi, and M.A.J. Mariscotti, Nucl. Phys. **A282**, 243 (1977).

[2] A.J. Kreiner, J. Davidson, M. Davidson, D. Abriola, C. Pomar, and P. Thieberger, Phys. Rev. C **36**, 2309 (1987); **37**, 1338 (1988).

[3] A.J. Kreiner and M.A.J. Mariscotti, Phys. Rev. Lett. **43**, 1150 (1979).

[4] A.J. Kreiner and M.A.J. Mariscotti, J. Phys. G **6**, 13 (1980).

[5] A.J. Kreiner, Z. Phys. A **288**, 373 (1978).

[6] R.A. Bark, J.M. Espino, W. Reviol, P.B. Semmes, H. Carlsson, I.G. Bearden, G.B. Hagemann, H.J. Jensen, I. Ragnarsson, L.L. Riedinger, H. Ryde, and P.O. Tjøm, Phys. Lett. B **406**, 193 (1997).

[7] M.A. Cardona, A.J. Kreiner, D. Hojman, G. Levinton, M.E. Debray, M. Davidson, J. Davidson, R. Pirchio, H. Somacal, D.R. Napoli, D. Bazzacco, N. Blasi, R. Burch, D. De Acuña, S.M. Lenzi, G. Lo Bianco, J. Rico, and C. Rossi Alvarez, Phys. Rev. C **59**, 1298 (1999).

[8] J.M. Espino, G.B. Hagemann, I.G. Bearden, R.A. Bark, M. Bergström, A. Bracco, B. Herskind, H.J. Jensen, S. Leoni, C. Martínez-Torre, B. Million, and P.O. Tjøm, Nucl. Phys. **A640**, 163 (1998).

[9] W. Reviol, L.L. Riedinger, X.Z. Wang, J.-Y. Zhang, H.J. Jensen, G.B. Hagemann, R.A. Bark, P.O. Tjøm, S. Leoni, T. Lönnroth, H. Schnack-Petersen, T. Shizuma, J. Wrzesinski, and P.B. Semmens, Phys. Rev. C **59**, 1351 (1999).

[10] S. Elfström, I. Forsblom, K. Fransson, L. Hildingsson, and W. Klamra, Z. Phys. A **305**, 87 (1982).

[11] S. Drissi, A. Bruder, M. Carlen, J.-Cl. Dousse, M. Gasser, J. Kern, S.J. Mannanal, B. Perny, Ch. Rhême, J.L. Salicio, J.P. Vorlet, and I. Hamamoto, Nucl. Phys. **A543**, 495 (1992).

[12] S.J. Mannanal, B. Boschung, M.W. Carlen, J.-Cl. Dousse, S. Drissi, P.E. Garrett, J. Kern, B. Perny, Ch. Rhême, J.P. Vorlet, C. Günthe, J. Manns, and U. Müller, Nucl. Phys. **A582**, 141 (1995).

[13] J.C. Walker and D.L. Harris, Phys. Rev. **121**, 224 (1961).

[14] J.C. Walker, Phys. Rev. **127**, 1739 (1962).

[15] K.-E. Ädelroth and C. Ekström, Nucl. Phys. **A198**, 380 (1972).

[16] G.D. Alkhazov, A.E. Barzakh, I.Ya. Chubukov, V.P. Denisov, V.S. Ivanov, V.N. Panteleev, V.E. Starodubsky, N.B. Buyanov, M.N. Fedoseyev, V.S. Letokhov, V.I. Mishin, and S.K. Sekatskii, Nucl. Phys. **A477**, 37 (1988).

[17] S. Drissi, S. André, D. Barnéoud, D. Foin, J. Genevey, and J.

Kern, Nucl. Phys. **A601**, 234 (1996).

[18] L.K. Peker, Nucl. Data Sheets **65**, 439 (1992).

[19] E.N. Shurshikov and N.V. Timofeeva, Nucl. Data Sheets **67**, 45 (1992).

[20] C.M. Baglin, Nucl. Data Sheets **90**, 431 (2000).

[21] B. Singh and A.R. Farhan, Nucl. Data Sheets **89**, 1 (2000).

[22] D. Bazzacco, Proceedings of the International Conference on Nuclear Structure at High Angular Momentum, Ottawa 1992, Report No. AECL 10613 (unpublished), Vol. 2, p. 376.

[23] F. Rösel, H.M. Fries, K. Alder, and H.C. Pauli, At. Data Nucl. Data Tables **21**, 293 (1978).

[24] K.E.G. Löbner, in *The Electromagnetic Interaction in Nuclear Spectroscopy*, edited by W.D. Hamilton (North-Holland, Amsterdam, 1975), p. 141.

[25] V.S. Shirley, Nucl. Data Sheets **64**, 505 (1991).

[26] C.J. Gallagher, Jr. and S.A. Moszkowski, Phys. Rev. **111**, 1282 (1958).

[27] F. Dönau and S. Frauendorf, in *Proceedings of the Conference on High Angular Momentum Properties of Nuclei*, Oak Ridge, USA, 1982, edited by N. Johnson (Harwood Academic, Chur, Switzerland, 1982), p. 143.

[28] D. Hojman, A.J. Kreiner, M. Davidson, J. Davidson, M. Debray, E.W. Cybulska, P. Pascholati, and W.A. Seale, Phys. Rev. C **45**, 90 (1992).

[29] S. Raman, C.H. Malarkey, W.T. Milner, C.W. Nestor, Jr., and P.H. Stelson, At. Data Nucl. Data Tables **36**, 1 (1987).

[30] A. Bohr and B. Mottelson, in *Nuclear Structure* (Benjamin, Reading, MA, 1975), Vol. 2.

[31] R. Bengtsson and S. Frauendorf, Nucl. Phys. **A327**, 139 (1979).

[32] E.N. Shurshikov and N.V. Timofeeva, Nucl. Data Sheets **65**, 365 (1992).

[33] H.J. Jensen, R.A. Bark, P.O. Tjøm, G.B. Hagemann, I.G. Bearden, H. Carlsson, S. Leoni, T. Lönnroth, W. Reviol, L.L. Riedinger, S. Schnack-Petersen, T. Shizuma, X.Z. Wang, and J. Wrzesinski, Nucl. Phys. **A695**, 3 (2001).

[34] R.A. Bark, H. Carlsson, S.J. Freeman, G.B. Hagemann, F. Ingebretsen, H.J. Jensen, T. Lönnroth, M.J. Piiparinen, I. Ragnarsson, H. Ryde, H. Schnack-Petersen, P.B. Semmes, and P.O. Tjøm, Nucl. Phys. **A630**, 603 (1998).

[35] F.R. Xu, W. Satula, and R. Wyss, Nucl. Phys. **A669**, 119 (2000).

[36] A.J. Kreiner, Phys. Rev. C **22**, 2570 (1980).

[37] J.P. Schiffer and W.W. True, Rev. Mod. Phys. **48**, 191 (1976).

[38] S. Ogaza, J. Kownacki, M.P. Carpenter, J. Gascon, G.B. Hagemann, Y. Iwata, H.J. Jensen, T. Komatsubara, J. Nyberg, G. Sletten, P.O. Tjøm, W. Waluś, and I. Hamamoto, Nucl. Phys. **A559**, 100 (1993).

[39] I. Hamamoto, J. Höller, and X.Z. Zhang, Phys. Lett. B **226**, 17 (1989).

[40] G.B. Hagemann, I. Hamamoto, and W. Satula, Phys. Rev. C **47**, 2008 (1993).

[41] A. Brockstedt, J. Lyttkens-Lindén, M. Bergström, L.P. Ekström, H. Ryde, J.C. Bacelar, J.D. Garrett, G.B. Hagemann, B. Herskind, F.R. May, P.O. Tjøm, and S. Frauendorf, Nucl. Phys. **A571**, 337 (1994).